universe

MDPI

Article

The Statistical Similarity of Repeating and Non-Repeating Fast Radio Bursts

Kongjun Zhang [1], Longbiao Li [2,*], Zhibin Zhang [1,*], Qinmei Li [1], Juanjuan Luo [3] and Min Jiang [1]

[1] Department of Physics, College of Physics, Guizhou University, Guiyang 550025, China; k_j_zhang@163.com (K.Z.); qinmli@163.com (Q.L.); j17385197986@163.com (M.J.)
[2] School of Mathematics and Physics, Hebei University of Engineering, Handan 056005, China
[3] College of Physics and Electronic Science, Qiannan Normal University, Duyun 55800, China; j_j_luo@sina.com
* Correspondence: lilongbiao@hebeu.edu.cn (L.L.); zbzhang@gzu.edu.cn (Z.Z.)

Abstract: In this paper, we present a sample of 21 repeating fast radio bursts (FRBs) detected by different radio instruments before September 2021. Using the Anderson–Darling test, we compared the distributions of extra-Galactic dispersion measure ($DM_{\rm E}$) of non-repeating FRBs, repeating FRBs and all FRBs. It was found that the $DM_{\rm E}$ values of three sub-samples are log-normally distributed. The $DM_{\rm E}$ of repeaters and non-repeaters were drawn from a different distribution on basis of the Mann–Whitney–Wilcoxon test. In addition, assuming that the non-repeating FRBs identified currently may be potentially repeators, i.e., the repeating FRBs to be universal and representative, one can utilize the averaged fluence of repeating FRBs as an indication from which to derive an apparent intensity distribution function (IDF) with a power-law index of $a_1 = 1.10 \pm 0.14$ ($a_2 = 1.01 \pm 0.16$, the observed fluence as a statistical variant), which is in good agreement with the previous IDF of 16 non-repeating FRBs found by Li et al. Based on the above statistics of repeating and non-repeating FRBs, we propose that both types of FRBs may have different cosmological origins, spatial distributions and circum-burst environments. Interestingly, the differential luminosity distributions of repeating and non-repeating FRBs can also be well described by a broken power-law function with the same power-law index of -1.4.

Keywords: high energy astrophysics (739); radio transient sources (2008); radio bursts (1339); extra-galactic radio sources (508); radio continuum emission (1340)

Citation: Zhang, K.; Li, L.; Zhang, Z.; Li, Q.; Luo, J.; Jiang, M. The Statistical Similarity of Repeating and Non-Repeating Fast Radio Bursts. *Universe* **2022**, *8*, 355. https://doi.org/10.3390/universe8070355

Academic Editor: Sergei B. Popov

Received: 4 May 2022
Accepted: 14 June 2022
Published: 27 June 2022

1. Introduction

Fast radio bursts (FRBs) are mysterious millisecond-duration radio pulses which occur randomly on the sky (e.g., [1–3]). FRBs were first found in archived pulsar survey data more than a decade ago [1], and more than 600 FRBs were reported as of April 2022 (e.g., [4–6]). However, the detection rate of FRBs is considered to be $\sim 10^3$–10^4 sky^{-1} day^{-1} [2,6–17], which means that FRBs are not uncommon in the Universe; e.g., 1652 repeating events from FRB 20121102A [18] and 1863 bursts from FRB 20201124A [19] were recently detected by the Five-hundred-meter Aperture Spherical radio Telescope (FAST, Li et al. [20]). The observed dispersion measures (DM) are larger than the DM contributions from the Milk Way (DM_{MW}) (except FRB 200428, which was confirmed to be from the Galactic magnetar SGR 1935+2154 [21–27]), which suggests an extragalactic, even cosmological origin in most cases.

It should be mentioned that there is no unambiguous physical origin for FRBs now. In general, FRBs' millisecond duration and high DM indicate the high brightness temperature (10^{32} K – 3.5×10^{35} K) [28] and the corresponding isotropic energy (E) released (10^{35} erg–10^{44} erg) [5,22,29,30]. Many progenitor models have been proposed to figure out what FRBs are (for a review, see, e.g., [31]), such as mergers of compact objects [32], flaring magnetars [33], young magnetars in supernova remnants [34], collisions between neutron star/magnetar and asteroids [35–39], collisions between episodic magnetic blobs [40], and

massive black hole model [41]. However, none of the current models can explain all the observational properties of FRBs. Fortunately, great progress in observations can help to constrain the progenitor model of FRBs; there has been a great leap forward in the research of FRBs. For example, the periodic activity of repeating FRB 20180916B suggests that the source is modulated by the orbital motion of a binary system [42]. Additionally, the discovery of Galactic FRB 200428 indicates the origin of a magnetar (e.g., [43]). In addition, some other models, e.g., the precession like a gyroscope model [43–47] and the spin period of isolated neutron star/magnetars model [48,49], can also work.

With the increase in FRBs monitoring by many radio telescopes, such as Very Large Array (VLA, Thompson et al. [50]), Australian Square Kilometer Array Pathfinder (ASKAP) [51], Canadian Hydrogen Intensity Mapping Experiment (CHIME, CHIME/FRB Collaboration et al. [52]) and FAST, it was found that some events are apparently "non-repeating," i.e., they did not repeat within a monitoring period. On the other hand, some sources have been repeating (e.g., [53–57]), which led to the successful identification of host galaxies and the precise mensuration of redshifts. Li et al. [5] analyzed 133 FRBs, including 110 non-repeating and 23 repeating ones, and proposed to classify FRBs into short and long groups according to pulse duration less than 100 ms or not. Interestingly, they found long FRBs are on average more energetic than short ones about two orders of magnitude. Moreover, they pointed out that FRBs could be used as a standard candle because peak luminosity becomes weakly dependent of the cosmological distance at higher redshift. Some observational properties of FRBs are similar to those of short and long gamma-ray bursts [58–60]. However, it is still uncertain whether this classification of FRBs is derived from the intrinsic physical characteristics, and whether repeating or "non-repeating" is due to observational selection bias—e.g., the monitor is not in the most active window for the "non-repeating" FRBs. Although the astrophysical origins of repeating and non-repeating FRBs are considered to be different (e.g., [61–64]), another viewpoint that most FRBs may be repeating sources has also been proposed [5,65–67]. It is now accepted that there are usually two types of FRBs, i.e., repeating FRBs and non-repeating FRBs. It is worth noting that the luminostiy function can place important constraints on the physical origins of FRBs and possible progenitors (e.g., [31,61,67–72]). Niino [69] has hypothesized three luminosity distribution function models (i.e., standard candle, power-law, and power-law + exponential cutoff) to investigate how differences in luminosity functions (LF) affect the observation properties of FRBs, and used the LF model and the cosmic FRB rate density to examine the distribution of $DM_{\rm E}$, the $\log N - \log S$ distribution, and the $DM_{\rm E} - S_{\rm peak}$ correlation. Luo et al. [61] constructed a Schechter luminosity function of 33 FRBs samples with a power-law index ranging from -1.8 to -1.2. Unfortunately, the LF of repeating FRBs has not been constructed yet due to the limit of numbers in the past. Hence, it is important and necessary to investigate their statistical characteristics and build the apparent intensity distribution function (IDF) and the LF of these repeating FRBs in order to disclose more natural differences from those non-repeating ones.

Our article is organized as follows. In Section 2, we introduce the FRB sample and present the statistical analyses of their parameters. The intensity distribution function of our repeating FRB sample is derived in Section 3. In Section 4, we construct the differential broken power-law LF of repeating FRBs and non-repeating FRBs based on the k-corrected isotropic luminosity (L). In Section 5, our conclusion and discussion are presented. The flat ΛCDM cosmological parameters $H_0 = 67.74\ {\rm km\,s^{-1}\ Mpc^{-1}}$, $\Omega_b = 0.0486$, $\Omega_m = 0.3089$, $\Omega_\Lambda = 0.6911$ have been adopted throughout the paper [73].

2. The Statistical Properties of Repeating FRBs

2.1. Distributions of Extra-Galactic Dispersion Measure and Total Energy

Currently, about 600 FRBs have been reported (including repeating bursts and apparent non-repeating bursts). Here, we collect the observation data of 21 repeating FRBs and 571 non-repeating FRBs. The sample of repeating FRBs was extracted from FRBCAT and several reported observational datasets (e.g., [53–56,74]). We list the key physical

parameters of 21 repeating FRBs in Table 1. It is worth mentioning that for the observed peak flux density ($S_{\rm peak}$) listed in Table 1, which is used as a representative of the brightness of an FRB, we chose the brightest one in every monitoring period for one repeating event. Additionally, the last column of Table 1 is the average fluence $\overline{F}$, which is calculated based on all archived observed fluence ($F_{\rm obs}$) for one repeating FRB. The reason is that multiple observations at different duty-circles inevitably suffer from the observational biases. Another reason is that number of sub-bursts within a repeater varies among distinct FRBs even for a comparable observation time, and thus is very difficult to count accurately. For instance, 1652 sub-bursts from FRB 20121102A [18] and 1863 sub-bursts from FRB 20201124A [19] were recently detected by FAST. In addition, the fluence fluctuations between different sub-bursts for one repeating FRB could be very large. For example, the fluences of FRB 20171019A were found to range from 0.37 to 388 Jy ms [56]. Although it is uncertain whether repeating or "non-repeating" is due to the observational select bias (e.g., [13,56,62] for a discussion of repeating FRBs), here we ignore the probability that the present non-repeating events may be found to be repeating in future, and treat them as real non-repeating events, whose corresponding parameters are not presented in the text because of their large number. Note that in Table 1, we consider the observed pulse width instead of the intrinsic one. The reason is that the intrinsic pulses of the narrow FRBs would be broadened due to scattering, and the scattering time scale is affected by the local environment of the FRB and is model-dependent, which results in a larger uncertainty. An appendix of non-repeating FRBs samples has been added separately at the end of the paper (for more details, see Table A1). Moreover, we did not consider FRB 200428 in our non-repeating burst sample, which is the only event detected in the Milky Way [21–23,25,75].

Table 1. Key physical parameters of 21 repeating FRBs before September 2021.

TNS Name	$\nu_{\rm c}$ [a] MHz	DM (pc cm^{-3})	DM_{MW} (pc cm^{-3})	$DM_{\rm E}$ [b] (pc cm^{-3})	$W_{\rm obs}$ (ms)	$S_{\rm peak}$ (Jy)	$F_{\rm obs}$ (Jy ms)	z	E (10^{39} erg)	$\overline{F}$ [d] (Jy ms)
FRB 20121102A	1375	557.00 ± 2.00	188.00	369.00	3.00 ± 0.50	$0.40^{+0.40}_{-0.10}$	$1.20^{+1.60}_{-0.55}$	0.31	0.13	0.36
FRB 20171019A	1297	460.80 ± 1.10	37.00	423.80	5.40 ± 0.30	40.50	219.00	0.35	34.01	101.62
FRB 20180814A	600	189.38 ± 0.09	87.00	102.38	2.60 ± 0.20	8.08 [c]	21.00	0.09	0.13	22.57
FRB 20180908B	600	195.70 ± 0.90	38.00	157.70	1.91 ± 0.10	0.60 ± 0.40	2.70	0.13	0.04	2.03
FRB 20180916B	600	349.70 ± 0.70	200.00	149.70	1.06 ± 0.05	7.64 [c]	8.10	0.12	0.12	10.26
FRB 20181017A	600	1281.00 ± 0.60	43.00	1238.00	20.20 ± 1.70	0.79 [c]	16.00	1.03	60.07	8.50
FRB 20181030A	600	103.50 ± 0.70	40.00	63.50	0.59 ± 0.08	12.37 [c]	7.30	0.05	0.02	4.75
FRB 20181119A	600	364.00 ± 0.30	34.00	330.00	2.66 ± 0.10	0.94 [c]	2.50	0.28	0.24	1.77
FRB 20181128A	600	450.20 ± 0.30	112.00	338.20	2.43 ± 0.16	1.81 [c]	4.40	0.28	0.46	3.45
FRB 20190116B	600	443.60 ± 0.80	20.00	423.60	1.50 ± 0.30	1.87 [c]	2.80	0.35	0.52	1.80
FRB20190117A	600	393.30 ± 0.10	48.00	345.30	1.44 ± 0.03	1.70 ± 0.60	5.90	0.29	0.64	6.36
FRB 20190208A	600	580.20 ± 0.20	72.00	508.20	1.31 ± 0.14	0.60 ± 0.30	2.00	0.42	0.60	1.70
FRB 20190209A	600	424.60 ± 0.60	46.00	378.60	3.70 ± 0.50	0.54 [c]	2.00	0.32	0.28	1.25
FRB 20190213A	600	651.50 ± 0.40	43.00	608.50	4.00	0.50 ± 0.30	3.00	0.51	1.46	1.80
FRB 20190212A	600	301.40 ± 0.20	49.00	252.40	2.10 ± 0.30	1.10 ± 0.60	2.50	0.21	0.13	2.67
FRB 20190222A	600	460.60 ± 0.10	87.00	373.60	2.97 ± 0.90	2.53 [c]	7.50	0.31	1.00	5.45
FRB 20190303A	600	221.80 ± 0.50	29.00	192.80	2.00 ± 0.30	0.50 ± 0.30	2.30	0.16	0.06	2.47
FRB 20190417A	600	1378.50 ± 0.30	78.00	1300.50	1.19 ± 0.02	0.70 ± 0.20	1.70	1.08	7.40	3.10
FRB 20190604A	600	552.60 ± 0.20	32.00	520.60	3.00 ± 0.40	0.90 ± 0.40	8.30	0.43	2.64	5.00
FRB 20190711A	23.8	593.10 ± 0.40	56.40	536.70	6.50 ± 0.50	5.23 [c]	34.00	0.45	9.88	17.70
FRB 20190907A	600	309.50 ± 0.30	53.00	256.50	0.54 ± 0.14	0.40 ± 0.20	0.90	0.21	0.05	1.10

Note: The all data were taken from http://www.frbcat.org [4] (accessed on 3 May 2022), and we report the properties of the brightest bursts for each repeater. [a] ν_c is the central frequency within the observational bandwith for an FRB. [b] $DM_{\rm E}$ is the extra-Galactic dispersion measure, which is defined as $DM_{\rm E} = DM - DM_{MW}$. [c] For $S_{\rm peak}$ which is not given in FRBCAT, the corresponding value is estimated by $S_{\rm peak} = F_{\rm obs}/W_{\rm obs}$. [d] $\overline{F}$ is the average fluence, which is calculated based on all archived $F_{\rm obs}$ of one repeating FRB.

The DM is a key quantity in the study of FRBs. CHIME/FRB Collaboration et al. [55] argued that FRBs can be divided into two subclasses (repeating and non-repeating FRBs)

according to the current observations. If repeating FRBs indeed differ from the apparent non-repeating FRBs—for example, the two subclasses have different host or local environments, or one population is intrinsically more bright—the DM distributions of the sub-samples could be obviously different. Meanwhile, their extra-Galactic dispersion measures ($DM_{\rm E} = DM - DM_{MW}$) could be distinctly distributed. We applied the Anderson–Darling (A–D) test to different kinds of FRBs, see Figure 1a,b, and list the statistical results in Table 2, where it is shown that the $DM_{\rm E}$ distributions of the non-repeating, repeating and all FRBs can be well described by a log-normal function. Furthermore, we found the mean values of $DM_{\rm E}$ are $496.9 \pm 16.9\,{\rm pc\,cm^{-3}}$ (0.70 dex) for non-repeating FRBs and $349.1 \pm 8.4\,{\rm pc\,cm^{-3}}$ (0.39 dex) for repeating FRBs via a Gauss fit. Simultaneously, we found that the mean values of $DM_{\rm E}$ of all FRBs are $485.1 \pm 15.2\,{\rm pc\,cm^{-3}}$ (0.67 dex). It is notable that the mean $DM_{\rm E}$ value of non-repeating FRBs is evidently larger than that of repeating FRBs. To check whether the $DM_{\rm E}$ distributions of non-repeaters and repeaters are same or not, we used a Mann–Whitney–Wilcoxon (M–W–W) test [76,77] and obtained the statistic $W = 4328.5$ with a p-value of 0.031, less than the significance threshold of 0.05, which demonstrates that the $DM_{\rm E}$ distributions of the two kinds of FRBs may have different progenitors or different physical mechanisms [31,64,78]. Notably, the $DM_{\rm E}$ is mainly contributed by the intergalactic medium, the host galaxies or the local environments. Unfortunately, what we have learned about the host galaxies is so little that the $DM_{\rm E}$ distributions are still uncertain and need to be verified by more observations in future.

In addition, we found that the radio energy of repeating FRBs ranges from 2.00×10^{37} to 6.01×10^{40} erg. We also used the Gauss function to fit the energy statistical distribution of repeating FRBs. As shown in panel Figure 1c, the total energy of repeating FRBs roughly follows a log-normal distribution with a mean value of $2.51^{+0.81}_{-0.59} \times 10^{38}$ erg and a scatter of 1.03 dex. Interesting, our result is roughly consistent with the early estimates of Li et al. [5] (10^{39}–10^{42} erg) for the repeating FRBs. Meanwhile, it is worth mentioning that this result is different from the bimodal energy distribution (a log-normal function and a generalized Cauchy function, with the peak of the energy distribution of 4.8×10^{37} erg) of a sub-sample of all the bursts from FRB 20121102A found by Li et al. [18] with FAST. Alternatively, it is possible that the bimodal energy distribution could be existent for a single burst but disappear when many bimodal distributions of diverse repeating FRBs are randomly mixed. However, Li et al. [5] noticed that the total energy of non-repeaters is on average larger than that of repeaters about one order of magnitude, which may demonstrate that at least some of repeating and non-repeating FRBs have different physical origins.

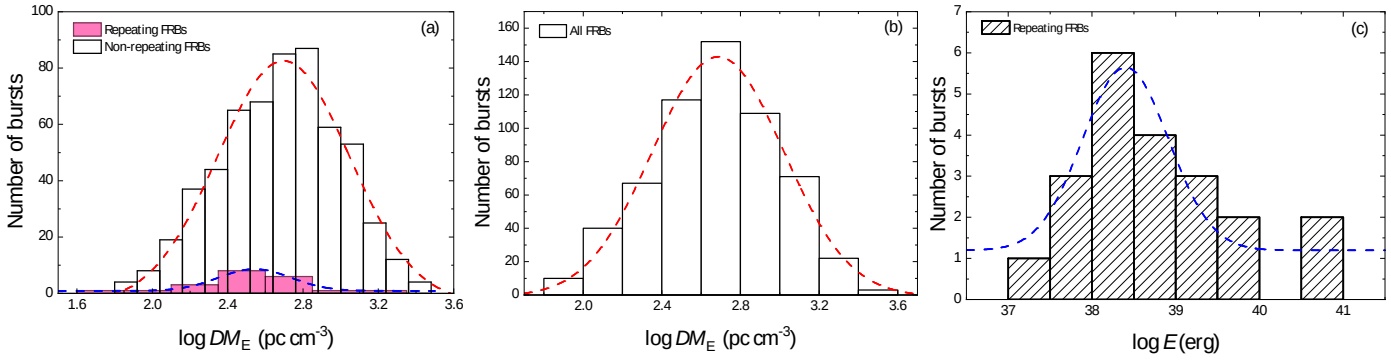

Figure 1. The logarithmic distributions of $DM_{\rm E}$ and radio energy of FRBs. Panel (**a**) presents the $DM_{\rm E}$ distributions of non-repeating and repeating FRBs and panel (**b**) displays the $DM_{\rm E}$ distributions of all FRBs. Panel (**c**) shows the radio energy distribution of repeating events. The dash lines are the best fits to data with a Gauss function.

Table 2. The statistical results of $DM_{\rm E}$ for non-repeating FRBs and repeating FRBs.

DM	FRB Sample	Statistic Value	The Critical Value	*p*-Value	Methods
DM_E	Non-repeating	0.814	1.084	0.035 [b]	A–D test [a]
DM_E	Repeating	0.427	0.963	0.285 [b]	A–D test [a]
DM_E	All	0.727	1.085	0.058 [b]	A–D test [a]
$DM_{\rm E}$	Repeating and Non-repeating FRBs	4328.5	...	0.031 [d]	M–W–W test [c]

[a] The A–D test was executed in logarithmic scale with a significance level of $\alpha = 0.01$. [b] A p-value larger than α indicates a log-normal distribution is favored [79]. [c] The M–W–W test was used to check different distributions with a significance Level of $\alpha = 0.05$. [d] A p-value greater than α means that the two distributions are the same [76].

2.2. Correlations between Some Characteristic Parameters

In Figure 2, the relationships of the $DM_{\rm E} - S_{\rm peak}, DM_{\rm E} - F_{\rm obs}, DM_{\rm E} - E$, $W_{\rm obs} - S_{\rm peak}, W_{\rm obs} - DM_{\rm E}, W_{\rm obs} - E$ of repeating FRBs are illustrated. Figure 2a shows that $S_{\rm peak}$ is not correlated with $DM_{\rm E}$. Note that the intrinsic width of the narrow FRBs is difficult to discern due to dispersion smearing and scattering broadening. Scattering is model dependent, and the assumptions of the model introduce high uncertainty. Therefore, we used the observed pulse width instead of the intrinsic pulse width in our work. Figure 2b shows that $F_{\rm obs}$ does not correlate with $DM_{\rm E}$. As shown in Figure 2c, the radio energy and the $DM_{\rm E}$ are positively correlated with a Pearson correlation coefficient of 0.81 and can be well-fitted. The power-law relation is $E \propto DM_{\rm E}^{2.60\pm0.04}$, which is roughly consistent with the tight correlation of non-repeating FRBs found by Li et al. [80], who argued that the positive correlation may be attributed to an observation selection effect—i.e., a fainter event is easier to be observed at a nearer distance. We found from Panels (d) and (e) that $W_{\rm obs}$ is not correlated with $S_{\rm peak}$ but obviously correlated with the $DM_{\rm E}$. Note that our $W_{\rm obs} - S_{\rm peak}$ relation is inconsistent with that of non-repeaters in [80]. The $S_{\rm peak}$ of the repeated FRBs spans three magnitudes and is more dispersive than the $S_{\rm peak}$ of the non-repeating FRBs sample of Li et al. [80], so that $W_{\rm obs}$ and $S_{\rm peak}$ are not correlated. Meanwhile, we found that there is a positive correlation between $W_{\rm obs}$ and the radio energy, as shown in Figure 2f. Li et al. [80] analyzed the correlations of key parameters of 16 non-repeating FRBs and found no clear correlation between energy and pulse width. For our repeating FRBs, the radio energy E and the pulse width $W_{\rm obs}$, respectively, span four and three orders of magnitude. The best-fitted power-law relation is $E \propto W_{\rm obs}^{0.43\pm0.06}$, with a correlation coefficient of 0.71 and a chance probability of 1.49×10^{-6}. This means that the repeating FRB pulse with a longer duration has a greater energy release generally, which is similar to those non-repeaters reported by Li et al. [80], and both of which are consistent with the findings in [5], where the averaged isotropic energies of long FRBs were found to be larger than those of short FRBs by at least two orders of magnitude, not only for non-repeating FRBs but also for repeating FRBs.

Figure 2e,f seems to show that $DM_{\rm E}$, $W_{\rm obs}$ and E may be related. This motivated us to perform multiple linear regression fitting for these three parameters in Figure 3. The three-parameter relation can be well described by a binary linear regression function as

$$\log E = (-1.31 \pm 0.97) + (1.85 \pm 0.41) \log DM_{\rm E} + (1.04 \pm 0.36) \log W_{\rm obs} \quad (1)$$

with a Pearson correlation coefficient of 0.88, which implies that wider FRBs usually hold larger energy outputs and higher DM_E values, and vice versa.

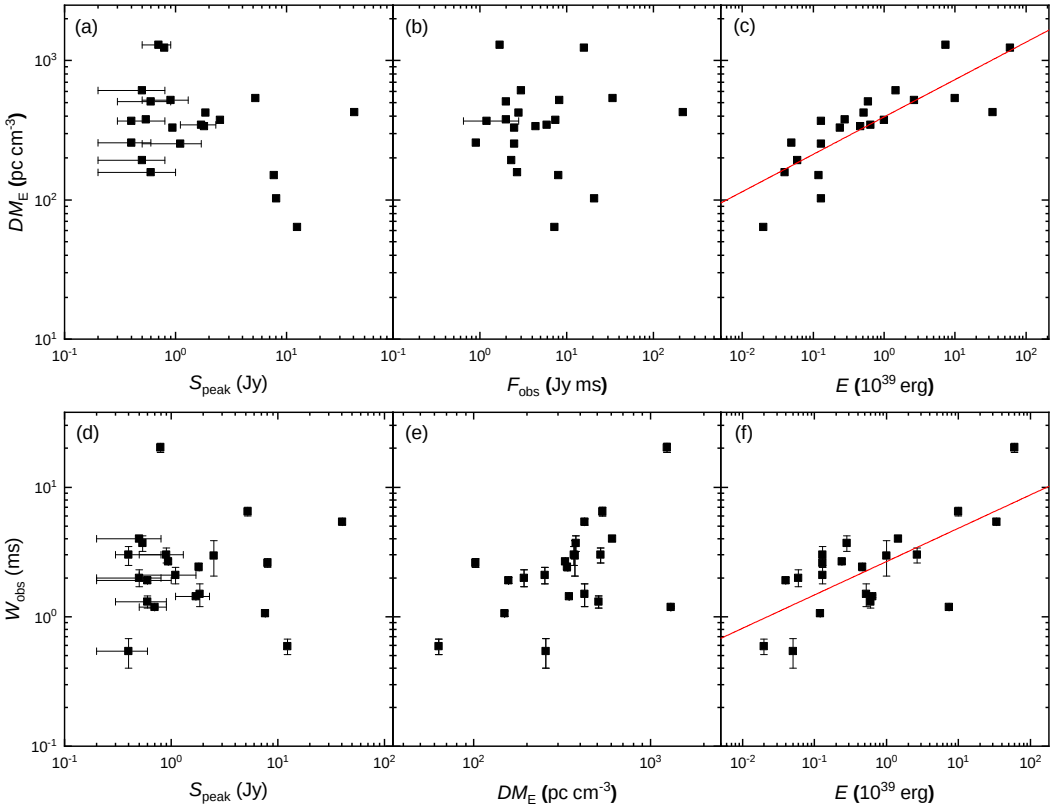

Figure 2. The correlations of DM_E with S_{peak}, F_{obs} and E are shown in Panels (**a**–**c**) respectively. The W_{obs} is plotted against S_{peak} in Panel (**d**), DM_E in Panel (**e**) and E in Panel (**f**). The observed data are symbolized with the filled squares. The solid lines in Panels (**c**,**f**) stand for the best fits to data with a power-law function.

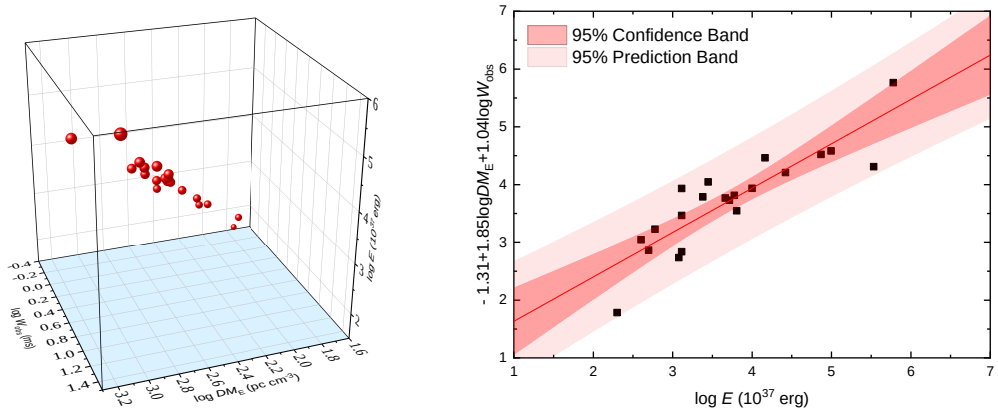

Figure 3. Left panel: Correlation among E, DM_E and W_{obs} of repeating FRBsis illustrated by the 3D scatter plot. Right panel: The isotropic energy E is plotted against the energy estimated by Equation (1). The solid line is the best fit to the data. The light and the heavy shaded regions are the 95% confidence and the 95% prediction ranges, respectively.

3. Apparent Intensity Distribution Function of Repeating FRBs

Li et al. [80] applied the F_{obs} of 16 non-repeating FRBs to derive an intensity distribution function (IDF). We considered the IDF of repeating FRBs to be determined by the average fluence ($\overline{F}$) and observed fluence (F_{obs}) of the brightest burst for each repeater. We then utilized the average fluence $\overline{F}$ presented in Table 1 to investigate the IDF of 21 repeating FRBs. This was done for several reasons: (1) For one repeating burst, multiple monitor observations in different time periods may lead to the observational bias. (2) The repeaters contain multiple bursts, and the number of monitored subbursts between

different repeaters varies—e.g., FAST has recently detected 1652 repeating events from FRB 20121102A [18] and 1863 bursts from FRB 20201124A [19]. (3) There is a certain degree of fluctuation between the fluences of repetitions for one repeating FRB; for example, the fluence of the repetitions from faint FRB 20171019A have a large range of 0.37 to ∼388 Jy ms [56]. Therefore, we took the mean fluence as a statistical variable for each repeater in order to build an apparent IDF of the repeating FRBs. In addition, we got rid of the faint FRB 20171019A from our repeating FRB sample because of its large fluctuations of fluence in the following calculations.

We assumed that FRBs can be considered as standard candles, and defined that the apparent IDF of repeating FRBs is in the same form as the function given by Li et al. [80]: $dN/dF_{\rm obs} = AF_{\rm obs}^{-a}$ (or $N(> F_{\rm obs}) \propto F_{\rm obs}^{-a+1}$), where α is the power-law index, $a = 2.5$ is expected for a uniform distribution and A is a constant which depends on the observations and the event rates of FRBs. We group the repeating FRB sample into several fluence intervals with a bin width of $\Delta\overline{F}$, and created the exemplary distributions of $\overline{F}$, as presented in Figure 4. Then we acquired a best-fit power-law curve for $dN/dF_{\rm obs}$. In Figure 4a, best fit results are shown for a bin width of $\Delta\overline{F} = 3.6$ Jy ms; the corresponding power-law index and the coefficient of determination (R-Square) are $a_1 = 1.07 \pm 0.05$ and 0.99, respectively. Note that the error bars along the x-axis and y-axis are, respectively, $\Delta\overline{F}/2$ and the square root of FRB count in each interval. Meanwhile, we also investigated the influence of bin width selection on the fitted results. In our work, the range of the bin width $\Delta\overline{F}$ was selected to be from 0.2 to 6.0 Jy ms, and the best-fit power-law indices corresponding to each $\Delta\overline{F}$ are shown in Figure 4b, where one can see that when $\Delta\overline{F}$ is in a range of 3.2–4.2 Jy ms, the fitted a_1 has smaller fluctuations and the corresponding error bar is also small. Hence, the a_1 values of $\Delta\overline{F} = 3.2 - 4.2$ Jy ms were selected to calculate the final average value, which is $a_1 = 1.10 \pm 0.14$. To constrain the unknown constant A, we adopted similar calculation processes to those described in detail in Li et al. [80] and compare them with the published event rates of FRBs in the literature in Table 3. The A value in our IDF was obtained to be $(2.37 \pm 0.76) \times 10^3\,\mathrm{sky}^{-1}\mathrm{day}^{-1}$. As a result, the final IDF of 20 repeating FRBs can be written as

$$\frac{dN}{dF} = (2.37 \pm 0.76) \times 10^3 F_{\rm obs}^{-1.10\pm0.14}\,\mathrm{sky}^{-1}\mathrm{day}^{-1}. \quad (2)$$

Similarly, we derived, while adopting $F_{\rm obs}$, the power-law $a_2 = 1.01 \pm 0.16$ of IDF for repeating FRBs (see Figure 4d). Furthermore, we got $A = (1.96 \pm 0.41) \times 10^3\,\mathrm{sky}^{-1}\mathrm{day}^{-1}$ for our IDF. The IDF of repeating FRBs is given by

$$\frac{dN}{dF} = (1.96 \pm 0.41) \times 10^3 F_{\rm obs}^{-1.01\pm0.16}\,\mathrm{sky}^{-1}\mathrm{day}^{-1}. \quad (3)$$

In particular, we found that power-law indices a_1 and a_2 have small differences, which indicates that our results are stable and reliable. If assuming the minimum fluence of 0.36 Jy ms as the threshold, one can estimate that the detection rate of repeating FRBs is at least $(9.64 \pm 3.09) \times 10^3$ sky^{-1} day^{-1} for a_1 and $(1.38 \pm 0.19) \times 10^4$ sky^{-1} day^{-1} for a_2. Combined with all parameters of FAST [81–83], we utilized the method of Li et al. [80], and estimate the detection rate for the 1000 h observation time is about 3 ± 1; that is slightly smaller than that for non-repeating FRBs predicted by Li et al. [80]. It is reasonable, since the current detection rate of non-repeating FRBs is obviously larger than that of repeating FRBs observationally.

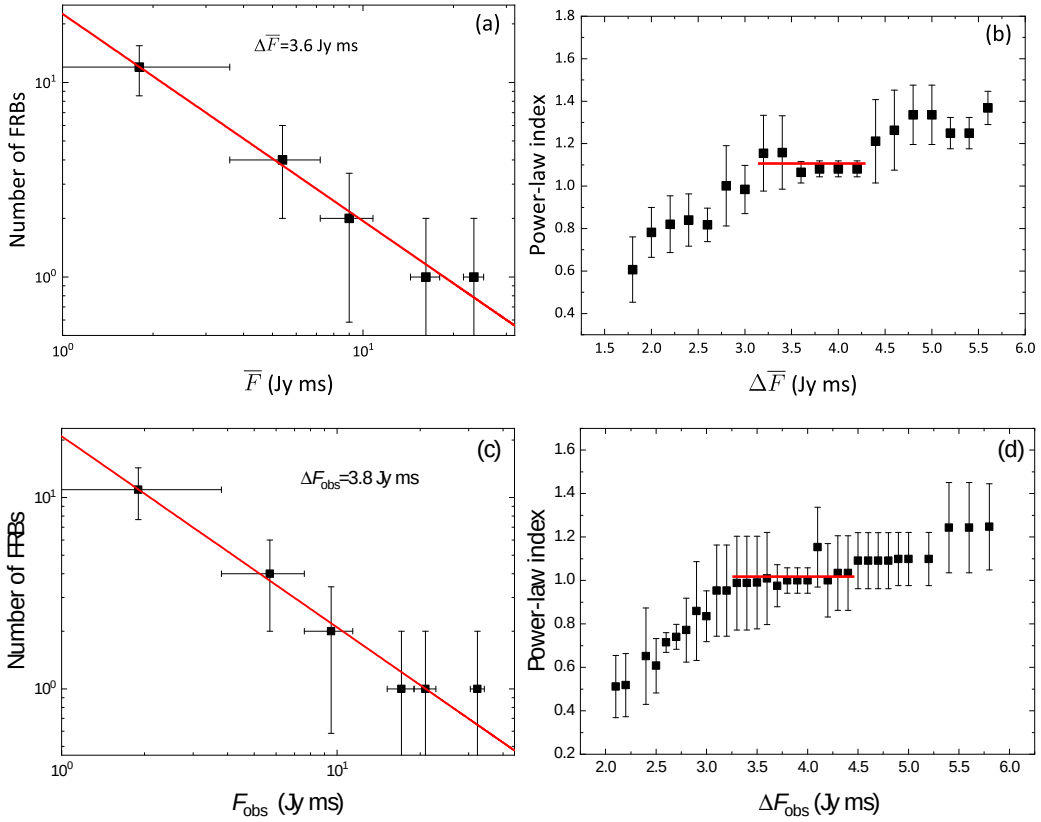

Figure 4. Panel (**a**) shows an exemplary distribution of $\overline{F}$ for a bin width of $\Delta\overline{F} = 3.6$ Jy ms. The solid line is the best-fit curve. Panel (**b**) illustrates the best-fit power-law values a_1 for each bin width; the solid short horizontal line shows the relatively stable range of $\Delta\overline{F} = 3.2$–4.2 Jy ms for a_1. Panel (**c**) shows an example distribution of $F_{\rm obs}$ for a bin width of $F_{\rm obs} = 3.8$ Jy ms. The solid line is the fitted curve. Panel (**d**) presents the best-fit power-law values a_2 for each bin width; the solid short horizontal line shows the relatively stable range of $\Delta F_{\rm obs} = 3.3$–4.4 Jy ms for a_2.

Table 3. Comparison of the deduced event rates of different FRB samples.

$F_{\rm Limit}$ (Jy ms)	$R(>F_{\rm Limit})$ (sky^{-1} day^{-1})	Reference	Coefficient A (10^3 sky^{-1} day^{-1})	FEB Class
3	$1.0^{+0.6}_{-0.5} \times 10^4$	Thornton et al. [2]	5.02 ± 1.62	non-repeaters
0.35	$3.1^{+12}_{-3.1} \times 10^4$	Spitler et al. [84]	7.49 ± 1.15	non-repeaters
2	2.5×10^3	Keane and Petroff [7]	1.06 ± 0.32	non-repeaters
1.8	1.2×10^4	Law et al. [8]	4.88 ± 1.38	non-repeaters
4	$4.4^{+5.2}_{-3.1} \times 10^3$	Rane et al. [11]	2.53 ± 0.87	non-repeaters
0.13–1.5	$7^{+5}_{-3} \times 10^3$	Champion et al. [9]	2.87 ± 0.82	non-repeaters
3.8	$3.3^{+3.7}_{-2.2} \times 10^3$	Crawford et al. [85]	1.85 ± 0.63	non-repeaters
0.03	$(3.03 \pm 1.56) \times 10^4$	Li et al. [80]	4.19 ± 0.22	non-repeaters
6	587	Lawrence et al. [86]	0.42 ± 0.16	non-repeaters
2	$1.7^{+1.5}_{-0.9} \times 10^3$	Bhandari et al. [12]	0.72 ± 0.21	non-repeaters
26	37 ± 8	Shannon et al. [15]	0.15 ± 0.01	non-repeaters
8	98^{+59}_{-39}	Farah et al. [16]	0.01 ± 0.003	non-repeaters
2	$3.4^{+15.4}_{-3.3} \times 10^3$	Parent et al. [17]	1.44 ± 0.42	non-repeaters
5	818 ± 64	CHIME/FRB Collaboration et al. [6]	0.53 ± 0.19	non-repeaters
0.36	$(9.64 \pm 3.09) \times 10^3$	this work	2.37 ± 0.76	repeaters

4. Differential Bolometric Luminosity Distributions

The luminosity functions of FRBs can be applied to reveal the origins of FRBs, design the optimal searching plan, guide future observations [61,67,80,87], etc. The detection

rate of the telescope can be calculated by the luminosity function, and the event rate density at different luminosity ranges sheds light on the origins of FRBs [31,78]. Building the LF requires not only the flux and distance, but also a k-correction of luminosity because of the different observational central frequencies (ν_c) in the mixed sample of FRBs. According to Zhang [29], the isotropic peak luminosity of a FRB can be calculated with $L_p \simeq 4\pi D_{\rm L}^2(z) S_{\rm peak} \nu_c$, where $D_{\rm L}(z)$ is the lumonisity distance calculated with the redshift given by FRBCAT (https://www.frbcat.org/). (accessed on 3 May 2022). We utilized ν_c to substitute the observational bandwidth of radio telescopes, which was proposed by Petroff et al. [4] and Aggarwal [88]. Additionally, Zhang [29] also suggested to use the central frequency instead of the receiver bandwidth since the FRB spectrum must be unknown and emissions may extend beyond the receiver bandwidth. In addition, when the observed flux densities of cosmological objects at different ν_c are considered, k-correction is also an important effect. After the k-correction, the bolometric luminosity can be given by $L \equiv L_p \simeq 4\pi D_{\rm L}^2(z) S_{\rm peak} \nu_c k$, in which the k-correction factor is taken as $k = (1+z)^{\alpha_t - \beta}$ with a temporal index of $\alpha_t \sim 0$ and a spectral index $\beta \sim 1/3$ [5,89], which are similar to those parameters of normal pulsar spectra [28,90,91].

The differential distributions of the k-corrected luminosity for 21 repeaters and 571 non-repeaters are shown in Figure 5, where one can notice that the repeaters are normally less luminous than the non-repeaters by about two orders of magnitude. Subsequently, we adopted a broken power-law from [92–94] to build the LF as

$$\phi(L) = \begin{cases} A\left(\frac{L}{L_{\rm b}}\right)^{\alpha_1}, & L \leq L_{\rm b} \\ A\left(\frac{L}{L_{\rm b}}\right)^{\alpha_2}, & L > L_{\rm b} \end{cases}, \tag{4}$$

where A is the normalized factor; L_b is the break luminosity; α_1 and α_2 are two power-law indices corresponding to lower and higher luminosity portions. In Figure 5, we can see that the luminosity distributions of both repeating and non-repeating FRBs can be well described by the broken power-law function, and the best-fit parameters are provided in Table 4. We excitingly found that the power-law indices of repeating and non-repeating bursts in the luminous end are the same as ≈ -1.4 within the range from -1.8 to -1.2, constrained by the Schechter luminosity function by Luo et al. [61]. However, we noticed that non-repeaters decline slower that repeaters in the less luminous end instead. In addition, after k-correction for observational frequency, the distributions of luminosity for repeating and non-repeating FRBs are similar at their brightest ends. The characteristic luminosity values L_b are not significantly different.

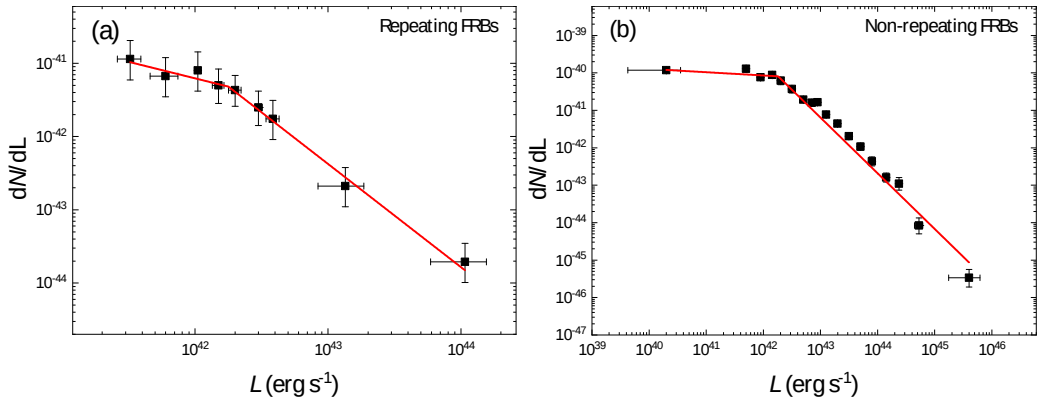

Figure 5. The luminosity functions of the repeating (Panel **a**) and non-repeating (Panel **b**) FRBs. The solid lines stand for the best fits with the power-law function of Equation (3). In each panel, the error bars along the x-axis are simply the standard errors in the corresponding luminosity bins, and the y-axis error bars are the 1-σ Poisson errors [95].

Table 4. The best-fit parameters of a broken power-law LF for repeating and non-repeating FRBs.

Sample	A	α_1	α_2	L_b (erg s^{-1})	χ^2_ν
Repeating FRBs	$(4.80 \pm 1.41) \times 10^{-42}$	-0.45 ± 0.20	-1.41 ± 0.08	$(1.78 \pm 0.44) \times 10^{42}$	0.17
Non-repeating FRBs	$(8.59 \pm 2.01) \times 10^{-41}$	-0.09 ± 0.10	-1.49 ± 0.05	$(1.74 \pm 0.29) \times 10^{42}$	3.17

5. Conclusions and Discussion

In this study, we analyzed the observed data of 21 repeating and 571 non-repeating FRBs published and drew the following conclusions:

- The extra-Galactic dispersion measures $DM_{\rm E}$ of non-repeating and repeating FRBs were found to be log-normally distributed with mean values of 496.9 pc cm^{-3} and 349.1 pc cm^{-3}, respectively. The M–W–W test showed that the $DM_{\rm E}$ is drawn from a different distribution.
- It was found that the total radio energies of repeating FRBs are log-normally distributed with a mean value of 2.51×10^{38} ergs (1.03 dex), which is smaller than to that of non-repeating FRBs, which is consistent with the conclusion in [5]. Surprisingly, the bimodal energy distribution discovered in FRB 20121102A by Li et al. [18] with FAST was not recovered in our repeating FRB sample any more.
- We statistically analyzed the relationships among $DM_{\rm E}$, $S_{\rm peak}$, $F_{\rm obs}$, E and $W_{\rm obs}$, and found that most correlations between them are similar to those of non-repeaters given by Li et al. [80], except that the $E - W_{\rm obs}$ relation of repeaters is tighter. The statistical results hint that the spatial distribution and the local environments of two samples of FRBs may be different, although more samples are needed to verify our argument, as noted by CHIME/FRB Collaboration et al. [55] and Fonseca et al. [74].
- We constructed a three-parameter relation to be $\log E \simeq -1.31 + 1.85 \log DM_{\rm E} + 1.04 \log W_{\rm obs}$, indicating that longer FRBs usually have larger extra-galactic dispersion measures and more energy releases, which supports the early findings by Li et al. [5], no matter whether a FRB is repeating or not.
- We assume that FRBs can be considered as standard candles homogeneously in a flat Euclidean space, with an IDF of $dN/dF_{\rm obs} = AF_{\rm obs}^{-a}$ (or $N(>F_{\rm obs}) \propto F_{\rm obs}^{-a+1}$), where a should be theoretically 2.5. Using the averaged fluence as a characteristic quantity, we built the IDF of repeating FRBs as $dN/dF = (2.37 \pm 0.76) \times 10^3 F_{\rm obs}^{-1.10 \pm 0.14}$ sky^{-1}day^{-1}. Likewise, using the observed fluence as a statistical indicator, we obtained the IDF as $dN/dF = (1.96 \pm 0.41) \times 10^3 F_{\rm obs}^{-1.01 \pm 0.16}$ sky^{-1}day^{-1}. The power-law index (a_1, a_2) of IDF deviates from the theoretical value of 2.5 in a flat Euclidean space, and shows that the repeating FRBs may be not uniformly distributed. Assuming the averaged minimum fluence as the threshold, we predicted the detection rate of repeaters to be about $(9.64 \pm 3.09) \times 10^3$ sky^{-1} day^{-1} or $(1.38 \pm 0.19) \times 10^4$ sky^{-1} day^{-1}; that is slightly lower in contrast with those non-repeating ones.
- Finally, we constructed and compared the luminosity functions of repeating and non-repeating FRBs. Interestingly, we found that the luminosity functions for both kinds of FRBs can be well characterized by a broken power-law relation; their power-law indices at their luminous ends are equal to ≈ -1.4, despite the discrepancy at their less-luminous ends.

Observationally, the power-law relation of $N \propto F^{\alpha}$, especially its power-law index a, indeed changes largely for different telescopes, owing to many factors, such as the selection effects/biases, the instrumental sensitivity, the sample incompleteness, the poor localizations, the small sample size or the cosmological effect (e.g., [12,90,96]), which may cause the relation to deviate from the theoretical form of $N \propto F^{-3/2}$ in a Euclidean space. Caleb et al. [68] pointed out by simulations that the slope of the logarithmic relation is mainly determined by cosmological effect and got $a = -0.9 \pm 0.3$, which matches a uniform distribution of FRBs roughly. Even for the same telescope, the deduced power-law indices could be inconsistent. For instance, Macquart and Ekers [90] found $a = -2.6^{+0.7}_{-1.3}$ and

James et al. [96] obtained $a = -1.18 \pm 0.24$ for Parkes FEBs. However, these power-law indices cannot show that the FRBs are not distributed in a Euclidean space. It is also why we took the average fluence as a characteristic quantity. Considering all above complex situations, we have assumed a universal slope in order to reduce the influences of uncertain factors on the $logN - logF$ relation.

In addition, we have constructed the luminosity functions for our samples of repeating and non-repeating FRBs on the basis of the k-corrected isotropic luminosities. It was found that the k-corrected luminosity of repeaters and non-repeaters span three and **six** orders of magnitude, respectively. On average, the repeaters are less energetic than the non-repeaters, which is coincident with [5]. The luminosity distributions of the two samples of FRBs can be well described by a broken power-law function with a break luminosity of $L_{\rm b} = 1.74 \times 10^{42}\,{\rm erg\,s^{-1}}$ for non-repeaters and $L_{\rm b} = 1.78 \times 10^{42}\,{\rm erg\,s^{-1}}$ for repeaters. This may imply that either repeaters or non-repeaters can be redivided into low- and high-luminosity types originating from different progenitors.

As addressed above, the $DM_{\rm E}$ distributions of the two samples have different distributions, which suggests that the majority of FRBs might have different astrophysical origins. Recent observations indicate that both kinds of FRBs may have distinct environments, such as dense, offset and star formation distribution (e.g., [97,98]). Additionally, there exist some special observed properties (such as polarization, rotation measures and the complex frequency–time structure) and a difference between FRB host galaxies [99–101]. Thus, these observational differences imply the emergence of subpopulations of FRBs. However, there are several recent works claiming no significant differences in the host galaxy properties (e.g., [102,103]). One possible reason is that the number of FRBs with known host galaxies is still limited currently. There is a debate about repeating and non-repeating (or more subclasses) or having a single population [62,104,105]. This means that the current classification results from the observations may be due to observational selection bias, e.g., if the observational period is not in the most active window for the individual FRBs [63,105], and one non-repeating burst identified currently may be a potential repeating FRB, as was the case for FRB 20171019A and FRB 20180301A. It may be just a few lucky cases, but we have probably missed many faint bursts of other FRBs. Nonetheless, the large sample of known FRBs is starting to show trends that suggest subclasses based on burst morphology and frequency–time structure (the downward frequency drift of sub-bursts [55,74,106], $\sim$100% linear polarization and negligible circular polarization [107]; and some sources show periodicity [108–110]). The observations in future should be focused on the FRB events which have relatively high probabilities of becoming repeating FRBs (see also [5]). When more FRBs are accurately localized, more useful information (such as DM, redshift, hosts and local environments of repeaters and apparently one-off FRBs) can be obtained from the direct observations, and the true LF will be accurately built as a cosmological probe to reveal the nature of FRBs.

Author Contributions: Conceptualization, Z.Z.; methodology, Z.Z. and L.L.; software, K.Z.; validation, K.Z., L.L. and Z.Z.; formal analysis, Z.Z.; investigation, K.Z.; resources, Z.Z.; data curation, Q.L., J.L. and M.J.; writing—original draft preparation, K.Z.; writing—review and editing, Z.Z. and L.L.; visualization, K.Z. and Q.L.; supervision, Z.Z.; project administration, Z.Z.; funding acquisition, Z.Z. Correspondence and requests for materials should be addressed to Z.Z. (zbzhang@gzu.edu.cn). All authors have read and agreed to the published version of the manuscript.

Funding: This research was funded by by the National Natural Science Foundation of China (grant numbers U2031118 and U1431126) and the science research grants from the China Manned Space Project, CMS-CSST-2021-B11. L. B. Li acknowledges support from the Natural Science Foundation of Hebei Province of China (grant number A2020402010). J. J. Luo acknowledges the Youth Science & Technology Talents Development Project of Guizhou Education Department (No.KY[2022]098).

Data Availability Statement: The data presented in this study are openly available in the following websites: https://www.frbcat.org/ and https://www.chime-frb.ca/catalog (accessed on 3 May 2022).

Acknowledgments: We appreciate the referees for their constructive and helpful comments and suggestions that have improved the paper greatly. This study was partly supported by the National Natural Science Foundation of China (grant numbers U2031118 and U1431126) and the science research grants from the China Manned Space Project, CMS-CSST-2021-B11. L. B. Li acknowledges support from the Natural Science Foundation of Hebei Province of China (grant number A2020402010). J. J. Luo acknowledges the Youth Science & Technology Talents Development Project of Guizhou Education Department (No.KY[2022]098).

Conflicts of Interest: The authors declare no conflict of interest.

Appendix A

The appendix Table A1 contains supplementary non-repeating FRBs details and data. Note: The FRBCAT sample were taken from FRB Catalogue [4] (https://www.frbcat.org/ (accessed on 3 May 2022)). CHIME samples of non-repeating FRBs were extracted from CHIME/FRB Catalog 1 [6] (https://www.chime-frb.ca/catalog (accessed on 3 May 2022)). The redshifts were calculated using the method of Petroff et al. [4] and Caleb et al. [68].

Table A1. Extended data.

TNS Name	ν_c (MHz)	DM (pc cm^{-3})	$DM_{\rm MW}$ (pc cm^{-3})	$DM_{\rm E}$ (pc cm^{-3})	$S_{\rm peak}$ (Jy ms)	z	$D_{\rm L}$ (Gpc)	$L_{\rm p}$ (erg s^{-1})
FRBCAT sample								
FRB 20010125A	1372.5	790.30	110.00	680.30	0.54	0.57	3.42	8.91×10^{42}
FRB 20010305A	1374	350.00	36.00	314.00	4.20	0.30	1.60	1.62×10^{43}
FRB 20010312A	1374	1187.00	51.00	1136.00	0.25	1.40	10.29	3.25×10^{43}
FRB 20010621A	1374	745.00	523.00	225.00	0.53	0.19	0.96	7.50×10^{41}
FRB 20010724A	1374	375.00	44.58	330.42	30.00	0.28	1.48	9.94×10^{43}
FRB 20090625A	1352	899.55	31.69	867.86	1.15	0.72	4.54	3.20×10^{43}
FRB 20110214A	1352	168.90	31.10	137.80	27.00	0.14	0.68	1.95×10^{43}
FRB 20110220A	1352	944.38	34.77	909.61	1.30	0.76	4.85	4.09×10^{43}
FRB 20110523A	800	623.30	43.52	579.78	0.60	0.48	2.78	3.89×10^{42}
FRB 20110626A	1352	723.00	47.46	675.54	0.63	0.56	3.34	9.83×10^{42}
FRB 20110703A	1352	1103.60	32.33	1071.27	0.50	0.89	5.88	2.27×10^{43}
FRB 20120127A	1352	553.30	31.82	521.48	0.62	0.43	2.44	5.29×10^{42}
FRB 20121002A	1352	1629.18	74.27	1554.91	0.76	1.30	9.39	8.21×10^{43}
FRB 20121029A	111	732.00	71.00	661.00	0.34	0.55	3.27	4.18×10^{41}
FRB 20130626A	1352	952.40	66.87	885.53	0.74	0.74	4.69	2.19×10^{43}
FRB 20130628A	1352	469.88	52.58	417.30	1.91	0.35	1.91	1.02×10^{43}
FRB 20130729A	1352	861.00	31.00	830.00	0.22	0.69	4.31	5.54×10^{42}
FRB 20131030A	111	203.00	64.40	138.60	0.24	0.12	0.58	1.03×10^{40}
FRB 20131104A	1352	779.00	71.10	707.90	1.16	0.59	3.56	2.04×10^{43}
FRB 20140212A	111	910.00	49.80	860.20	0.26	0.72	4.54	5.93×10^{41}
FRB 20140514A	1352	562.70	34.90	527.80	0.47	0.44	2.51	4.24×10^{42}
FRB 20141113A	1375	400.30	188.00	212.30	0.04	0.15	0.74	3.32×10^{40}
FRB 20141216A	111	545.00	69.50	475.50	0.23	0.40	2.24	1.37×10^{41}
FRB 20150215A	1352	1105.60	427.20	678.40	0.70	0.57	3.42	1.14×10^{43}
FRB 20150418A	1352	776.20	188.50	587.70	2.20	0.49	2.85	2.53×10^{43}
FRB 20150610A	1352	1593.90	122.00	1471.90	0.70	1.20	8.51	6.30×10^{43}
FRB 20150807A	1352	266.50	36.90	229.60	128.00	0.19	0.96	1.78×10^{44}
FRB 20151018A	111	570.00	275.00	295.00	1.40	0.24	1.24	2.67×10^{41}
FRB 20151125A	2.5	273.00	50.20	222.80	0.54	0.19	0.96	1.39×10^{39}
FRB 20151206A	1352	1909.80	160.00	1749.80	0.30	1.50	11.20	4.48×10^{43}
FRB 20151230A	1352	960.40	38.00	922.40	0.42	0.80	5.16	1.49×10^{43}
FRB 20160102A	1352	2596.10	13.00	2583.10	0.50	2.10	16.91	1.59×10^{44}
FRB 20160206A	111	1262.00	69.10	1192.90	0.26	0.99	6.71	1.24×10^{42}
FRB 20160317A	843	1165.00	319.60	845.40	3.00	0.70	4.38	4.87×10^{43}
FRB 20160410A	843	278.00	57.70	220.30	7.00	0.18	0.90	5.41×10^{42}
FRB 20160608A	843	682.00	238.30	443.70	4.30	0.37	2.04	1.63×10^{43}
FRB 20160920A	111	1767.00	250.00	1517.00	0.22	1.20	8.51	1.63×10^{42}
FRB 20161202A	111	291.00	69.80	221.20	0.29	0.18	0.90	2.95×10^{40}

Table A1. *Cont.*

TNS Name	ν_c (MHz)	DM (pc cm^{-3})	$DM_{\rm MW}$ (pc cm^{-3})	$DM_{\rm E}$ (pc cm^{-3})	$S_{\rm peak}$ (Jy ms)	z	$D_{\rm L}$ (Gpc)	$L_{\rm p}$ (erg s^{-1})
FRB 20170107A	1320	609.50	35.00	574.50	24.10	0.48	2.78	2.58×10^{44}
FRB 20170416A	1320	523.20	40.00	483.20	19.40	0.40	2.24	1.37×10^{44}
FRB 20170428A	1320	991.70	40.00	951.70	7.70	0.79	5.08	2.59×10^{44}
FRB 20170606A	111	247.00	250.00	(3.00)	0.54	0.06	0.26	4.87×10^{39}
FRB 20170707A	1297	235.20	36.00	199.20	14.80	0.17	0.84	1.56×10^{43}
FRB 20170712A	1297	312.79	38.00	274.79	37.80	0.23	1.18	7.66×10^{43}
FRB 20170827A	835	176.80	37.00	139.80	60.00	0.12	0.58	1.93×10^{43}
FRB 20170906A	1297	390.30	39.00	351.30	29.60	0.29	1.54	1.00×10^{44}
FRB 20170922A	835	1111.00	45.00	1066.00	5.19	1.20	8.51	2.88×10^{44}
FRB 20171003A	1297	463.20	40.00	423.20	40.50	0.35	1.91	2.08×10^{44}
FRB 20171004A	1297	304.00	38.00	266.00	22.00	0.22	1.13	4.05×10^{43}
FRB 20171019A	1297	114.10	38.00	76.10	117.60	0.06	0.28	1.38×10^{43}
FRB 20171020A	1297	618.50	36.00	582.50	19.60	0.49	2.85	2.16×10^{44}
FRB 20171116A	1352	1457.40	13.00	1444.40	1.48	1.57	11.85	2.45×10^{44}
FRB 20171209A	1297	158.60	36.00	122.60	88.60	0.10	0.48	3.01×10^{43}
FRB 20171213A	1297	203.10	37.00	166.10	21.00	0.14	0.68	1.45×10^{43}
FRB 20171216A	1297	715.70	38.00	677.70	128.10	0.56	3.34	1.92×10^{45}
FRB 20180110A	1297	402.70	36.00	366.70	40.70	0.31	1.66	1.60×10^{44}
FRB 20180119A	1297	441.40	32.00	409.40	17.50	0.34	1.85	8.44×10^{43}
FRB 20180128B	1297	495.90	40.00	455.90	28.70	0.38	2.11	1.78×10^{44}
FRB 20180130A	1297	343.50	39.00	304.50	23.10	0.25	1.30	5.62×10^{43}
FRB 20180131A	1297	657.70	40.00	617.70	22.20	0.51	2.99	2.68×10^{44}
FRB 20180212A	1297	167.50	33.00	134.50	53.00	0.11	0.53	2.20×10^{43}
FRB 20180309A	1352	263.42	44.69	218.73	27.60	0.19	0.96	3.84×10^{43}
FRB 20180311A	1352	1570.90	45.20	1530.40	0.20	2.00	15.94	5.70×10^{43}
FRB 20180315A	1297	479.00	36.00	443.00	23.30	0.37	2.04	1.36×10^{44}
FRB 20180321A	111	594.00	70.00	524.00	0.54	0.44	2.51	3.99×10^{41}
FRB 20180324A	1297	431.00	70.00	361.00	16.50	0.30	1.60	6.02×10^{43}
FRB 20180417A	1272.5	474.80	26.15	448.65	21.80	0.37	2.04	1.25×10^{44}
FRB 20180430A	1297	264.10	165.44	98.66	147.50	0.08	0.38	3.14×10^{43}
FRB 20180515A	1320	355.20	33.00	322.20	24.20	0.20	1.01	3.68×10^{43}
FRB 20180525A	1297	388.10	31.00	357.10	78.90	0.30	1.60	2.88×10^{44}
FRB 20180528A	835	899.30	69.00	830.30	15.75	0.90	5.97	4.52×10^{44}
FRB 20180714A	1352	1467.92	257.00	1212.87	5.00	1.60	12.12	8.65×10^{44}
FRB 20180725A	400	715.98	71.00	644.98	38.71	0.54	3.20	1.64×10^{44}
FRB 20180727A	600	642.07	21.00	621.07	17.95	0.52	3.06	1.05×10^{44}
FRB 20180729B	600	317.37	95.00	222.37	112.50	0.19	0.96	6.96×10^{43}
FRB 20180729A	600	109.61	31.00	78.61	283.33	0.07	0.33	2.11×10^{43}
FRB 20180730A	600	849.05	57.00	792.05	119.05	0.66	4.08	1.20×10^{45}
FRB 20180801A	600	656.20	90.00	566.20	54.90	0.47	2.71	2.55×10^{44}
FRB 20180806A	600	739.98	41.00	698.98	34.78	0.58	3.49	2.61×10^{44}
FRB 20180810A	600	414.95	104.00	310.95	40.74	0.26	1.36	5.00×10^{43}
FRB 20180810B	600	169.13	47.00	122.13	60.71	0.10	0.48	9.54×10^{42}
FRB 20180812A	600	802.57	83.00	719.57	14.40	0.60	3.63	1.17×10^{44}
FRB 20180814B	600	238.32	41.00	197.32	138.89	0.16	0.79	5.92×10^{43}
FRB 20180817A	600	1006.84	28.00	978.84	75.68	0.82	5.32	1.26×10^{45}
FRB 20180924B	1320	361.42	40.50	320.92	12.30	0.34	1.85	6.04×10^{43}
FRB 20181016A	835	1982.80	90.00	1892.80	10.19	2.20	17.90	2.21×10^{45}
FRB 20181017C	835	239.97	38.00	201.97	161.00	0.20	1.01	1.55×10^{44}
FRB 20181112A	1272.5	589.27	102.00	487.27	12.38	0.41	2.31	8.93×10^{43}
FRB 20181123B	1250	1812.00	149.50	1662.50	0.07	1.39	10.20	7.56×10^{42}
FRB 20181228D	835	354.20	58.00	296.20	19.23	0.30	1.60	4.51×10^{43}
FRB 20190102C	1320	363.60	57.30	306.30	8.24	0.26	1.36	2.23×10^{43}
FRB 20190523A	1411	760.80	37.00	723.80	666.67	0.60	3.63	1.27×10^{46}
FRB 20190608B	1320	338.70	37.20	301.50	4.33	0.25	1.30	1.07×10^{43}
FRB 20190611B	1320	321.40	57.83	263.57	5.00	0.22	1.13	9.36×10^{42}
FRB 20191108A	1370	588.10	52.00	536.10	27.00	0.52	3.06	3.60×10^{44}
FRB 20190614D	1400	959.20	83.50	875.70	0.12	0.73	4.61	3.68×10^{42}
FRB 20200125A	350	179.47	25.00	154.47	0.37	0.17	0.84	1.04×10^{41}

Table A1. *Cont.*

TNS Name	ν_c (MHz)	DM (pc cm^{-3})	$DM_{\rm MW}$ (pc cm^{-3})	$DM_{\rm E}$ (pc cm^{-3})	$S_{\rm peak}$ (Jy ms)	z	$D_{\rm L}$ (Gpc)	$L_{\rm p}$ (erg s^{-1})
CHIME sample								
FRB20180725A	600	715.81	71.61	644.20	1.70	0.54	3.18	1.07×10^{43}
FRB20180727A	600	642.13	21.23	620.90	0.58	0.52	3.04	3.35×10^{42}
FRB20180729A	600	109.59	30.79	78.80	11.70	0.07	0.30	7.65×10^{41}
FRB20180729B	600	317.22	94.02	223.20	0.92	0.19	0.93	5.43×10^{41}
FRB20180730A	600	848.90	59.20	789.70	5.20	0.66	4.07	5.22×10^{43}
FRB20180801A	600	655.73	90.13	565.60	1.11	0.47	2.72	5.18×10^{42}
FRB20180806A	600	739.95	40.65	699.30	1.90	0.58	3.51	1.44×10^{43}
FRB20180810A	600	414.88	104.68	310.20	1.10	0.26	1.35	1.33×10^{42}
FRB20180810B	600	169.14	45.84	123.30	5.20	0.10	0.49	8.65×10^{41}
FRB20180812A	600	802.45	80.35	722.10	0.93	0.60	3.65	7.59×10^{42}
FRB20180814B	600	238.35	41.15	197.20	3.40	0.16	0.81	1.54×10^{42}
FRB20180817A	600	1006.77	27.67	979.10	2.40	0.82	5.29	3.95×10^{43}
FRB20180904A	600	361.14	55.44	305.70	3.80	0.25	1.33	4.46×10^{42}
FRB20180906A	600	383.46	43.46	340.00	1.60	0.28	1.50	2.38×10^{42}
FRB20180906B	600	3038.06	31.36	3006.70	0.36	2.51	20.96	7.48×10^{43}
FRB20180907A	600	877.24	92.04	785.20	0.87	0.65	4.04	8.61×10^{42}
FRB20180907B	600	658.19	38.09	620.10	1.08	0.52	3.04	6.22×10^{42}
FRB20180907C	600	638.20	91.40	546.80	1.11	0.46	2.61	4.80×10^{42}
FRB20180907D	600	1447.10	56.00	1391.10	0.89	1.16	8.15	3.28×10^{43}
FRB20180907E	600	383.36	30.46	352.90	0.73	0.29	1.57	1.18×10^{42}
FRB20180909A	600	408.65	49.85	358.80	0.33	0.30	1.60	5.53×10^{41}
FRB20180910A	600	684.41	58.11	626.30	6.50	0.52	3.07	3.83×10^{43}
FRB20180911A	600	221.25	56.55	164.70	1.60	0.14	0.67	4.92×10^{41}
FRB20180915A	600	371.03	171.93	199.10	2.30	0.17	0.82	1.06×10^{42}
FRB20180915B	600	177.13	22.43	154.70	0.99	0.13	0.62	2.66×10^{41}
FRB20180916A	600	296.03	78.43	217.60	2.40	0.18	0.91	1.34×10^{42}
FRB20180916C	600	2252.87	73.87	2179.00	0.39	1.82	14.16	3.98×10^{43}
FRB20180917B	600	857.04	43.14	813.90	1.03	0.68	4.22	1.11×10^{43}
FRB20180918A	600	1453.99	79.99	1374.00	1.45	1.15	8.03	5.20×10^{43}
FRB20180919B	600	560.22	32.82	527.40	2.56	0.44	2.50	1.02×10^{43}
FRB20180920A	600	555.66	160.76	394.90	0.86	0.33	1.78	1.78×10^{42}
FRB20180920B	600	463.40	33.20	430.20	0.35	0.36	1.97	8.80×10^{41}
FRB20180921A	600	394.37	35.17	359.20	0.92	0.30	1.60	1.54×10^{42}
FRB20180922A	600	555.69	141.29	414.40	2.60	0.35	1.88	6.01×10^{42}
FRB20180923A	600	219.44	100.04	119.40	0.76	0.10	0.47	1.18×10^{41}
FRB20180923C	600	173.98	29.08	144.90	0.89	0.12	0.58	2.08×10^{41}
FRB20180923D	600	329.40	30.70	298.70	2.40	0.25	1.29	2.68×10^{42}
FRB20180924A	600	1116.55	69.25	1047.30	1.30	0.87	5.74	2.50×10^{43}
FRB20180925A	600	237.74	70.64	167.10	0.99	0.14	0.68	3.14×10^{41}
FRB20180925B	600	667.87	39.67	628.20	0.76	0.52	3.08	4.51×10^{42}
FRB20180928A	600	252.77	158.07	94.70	1.34	0.08	0.37	1.28×10^{41}
FRB20181012B	600	715.19	33.49	681.70	0.49	0.57	3.40	3.51×10^{42}
FRB20181013A	600	309.31	48.11	261.20	2.81	0.22	1.11	2.34×10^{42}
FRB20181013B	600	277.51	85.81	191.70	0.56	0.16	0.79	2.38×10^{41}
FRB20181013C	600	1005.77	38.57	967.20	0.44	0.81	5.21	7.04×10^{42}
FRB20181013E	600	345.30	80.80	264.50	0.62	0.22	1.13	5.30×10^{41}
FRB20181014A	600	1314.89	186.69	1128.20	0.99	0.94	6.30	2.26×10^{43}
FRB20181014B	600	887.97	102.57	785.40	0.65	0.65	4.04	6.44×10^{42}
FRB20181014C	600	752.17	59.87	692.30	0.57	0.58	3.47	4.22×10^{42}
FRB20181014D	600	377.13	30.03	347.10	8.40	0.29	1.54	1.31×10^{43}
FRB20181015A	600	568.82	46.52	522.30	1.51	0.44	2.47	5.88×10^{42}
FRB20181017B	600	307.37	43.67	263.70	1.06	0.22	1.12	9.00×10^{41}
FRB20181018A	600	1129.45	120.95	1008.50	0.49	0.84	5.48	8.63×10^{42}
FRB20181018B	600	293.87	113.17	180.70	5.10	0.15	0.74	1.91×10^{42}
FRB20181018C	600	411.19	146.19	265.00	2.40	0.22	1.13	2.06×10^{42}

Table A1. *Cont.*

TNS Name	ν_c (MHz)	DM (pc cm^{-3})	DM_{MW} (pc cm^{-3})	DM_{E} (pc cm^{-3})	S_{peak} (Jy ms)	z	D_{L} (Gpc)	L_{p} (erg s^{-1})
FRB20181019B	600	725.18	159.78	565.40	0.72	0.47	2.72	3.36×10^{42}
FRB20181019C	600	501.64	39.24	462.40	1.16	0.39	2.14	3.43×10^{42}
FRB20181020A	600	1112.47	72.17	1040.30	0.80	0.87	5.70	1.51×10^{43}
FRB20181022C	600	528.47	49.87	478.60	0.91	0.40	2.23	2.91×10^{42}
FRB20181022D	600	514.33	20.13	494.20	2.90	0.41	2.32	9.97×10^{42}
FRB20181022E	600	285.99	21.79	264.20	0.69	0.22	1.13	5.88×10^{41}
FRB20181025A	600	592.56	61.66	530.90	1.52	0.44	2.52	6.14×10^{42}
FRB20181027A	600	727.74	64.04	663.70	4.90	0.55	3.29	3.30×10^{43}
FRB20181030C	600	668.76	73.06	595.70	1.60	0.50	2.89	8.41×10^{42}
FRB20181030D	600	289.44	123.54	165.90	2.74	0.14	0.67	8.55×10^{41}
FRB20181030E	600	159.69	49.89	109.80	2.00	0.09	0.43	2.61×10^{41}
FRB20181101A	600	1472.68	144.88	1327.80	0.50	1.11	7.70	1.66×10^{43}
FRB20181102A	600	414.46	155.66	258.80	1.48	0.22	1.10	1.21×10^{42}
FRB20181104C	600	580.82	105.32	475.50	9.70	0.40	2.21	3.05×10^{43}
FRB20181115A	600	981.61	40.01	941.60	0.44	0.78	5.04	6.62×10^{42}
FRB20181116A	600	355.43	37.13	318.30	4.00	0.27	1.39	5.13×10^{42}
FRB20181116B	600	409.88	36.38	373.50	0.74	0.31	1.67	1.36×10^{42}
FRB20181117A	600	959.28	38.08	921.20	0.61	0.77	4.91	8.72×10^{42}
FRB20181117B	600	538.20	65.00	473.20	3.60	0.39	2.20	1.12×10^{43}
FRB20181117C	600	1773.74	66.14	1707.60	1.57	1.42	10.50	9.24×10^{43}
FRB20181118A	600	557.41	31.51	525.90	4.30	0.44	2.49	1.70×10^{43}
FRB20181118B	600	422.28	53.08	369.20	0.78	0.31	1.65	1.39×10^{42}
FRB20181119B	600	609.10	442.30	166.80	4.50	0.14	0.68	1.42×10^{42}
FRB20181119C	600	284.96	44.66	240.30	2.80	0.20	1.01	1.94×10^{42}
FRB20181119E	600	1169.77	220.27	949.50	0.70	0.79	5.09	1.07×10^{43}
FRB20181122A	600	662.82	196.12	466.70	0.53	0.39	2.17	1.60×10^{42}
FRB20181122B	600	225.76	54.36	171.40	14.70	0.14	0.70	4.92×10^{42}
FRB20181123A	600	798.72	103.82	694.90	0.99	0.58	3.48	7.40×10^{42}
FRB20181124A	600	1108.53	34.43	1074.10	0.66	0.90	5.93	1.34×10^{43}
FRB20181124B	600	801.64	104.94	696.70	2.61	0.58	3.49	1.96×10^{43}
FRB20181125A	600	272.19	37.99	234.20	0.39	0.20	0.98	2.56×10^{41}
FRB20181126A	600	494.22	49.62	444.60	3.50	0.37	2.05	9.47×10^{42}
FRB20181127A	600	930.32	32.22	898.10	0.78	0.75	4.76	1.05×10^{43}
FRB20181128B	600	456.55	33.55	423.00	0.34	0.35	1.93	8.23×10^{41}
FRB20181128C	600	618.35	49.15	569.20	0.39	0.47	2.74	1.85×10^{42}
FRB20181128D	600	146.50	32.70	113.80	2.60	0.09	0.45	3.65×10^{41}
FRB20181129A	600	385.97	86.77	299.20	1.52	0.25	1.30	1.70×10^{42}
FRB20181129B	600	405.91	62.11	343.80	4.00	0.29	1.52	6.09×10^{42}
FRB20181129C	600	502.22	26.52	475.70	0.77	0.40	2.22	2.43×10^{42}
FRB20181130A	600	220.09	95.09	125.00	0.97	0.10	0.50	1.66×10^{41}
FRB20181201A	600	694.36	23.96	670.40	0.40	0.56	3.33	2.75×10^{42}
FRB20181201B	600	876.58	51.28	825.30	0.66	0.69	4.29	7.33×10^{42}
FRB20181202A	600	667.95	38.75	629.20	2.63	0.52	3.09	1.57×10^{43}
FRB20181202B	600	825.88	33.68	792.20	0.99	0.66	4.08	1.00×10^{43}
FRB20181202C	600	557.16	126.46	430.70	0.51	0.36	1.97	1.29×10^{42}
FRB20181203A	600	635.93	46.73	589.20	1.74	0.49	2.86	8.92×10^{42}
FRB20181203B	600	375.39	56.69	318.70	1.45	0.27	1.39	1.87×10^{42}
FRB20181203C	600	2444.57	37.47	2407.10	1.05	2.01	15.99	1.34×10^{44}
FRB20181208A	600	562.78	45.18	517.60	0.95	0.43	2.45	3.63×10^{42}
FRB20181209A	600	328.66	65.66	263.00	2.50	0.22	1.12	2.11×10^{42}
FRB20181213A	600	678.67	48.57	630.10	0.88	0.53	3.09	5.26×10^{42}
FRB20181213B	600	626.59	30.59	596.00	0.75	0.50	2.90	3.95×10^{42}
FRB20181213C	600	380.74	30.54	350.20	0.62	0.29	1.55	9.84×10^{41}
FRB20181214A	600	468.15	184.25	283.90	0.16	0.24	1.22	1.56×10^{41}

Table A1. *Cont.*

TNS Name	ν_c (MHz)	DM (pc cm^{-3})	DM_{MW} (pc cm^{-3})	DM_{E} (pc cm^{-3})	S_{peak} (Jy ms)	z	D_{L} (Gpc)	L_{p} (erg s^{-1})
FRB20181214B	600	1120.75	42.05	1078.70	0.41	0.90	5.96	8.43×10^{42}
FRB20181214C	600	632.78	33.28	599.50	1.20	0.50	2.92	6.40×10^{42}
FRB20181214D	600	1177.32	26.02	1151.30	0.55	0.96	6.45	1.31×10^{43}
FRB20181214F	600	2105.76	40.26	2065.50	0.31	1.72	13.26	2.80×10^{43}
FRB20181215A	600	412.63	128.53	284.10	0.34	0.24	1.22	3.40×10^{41}
FRB20181215B	600	494.01	40.61	453.40	1.90	0.38	2.09	5.37×10^{42}
FRB20181216A	600	542.74	146.74	396.00	0.94	0.33	1.79	1.96×10^{42}
FRB20181217A	600	1177.17	69.77	1107.40	0.64	0.92	6.15	1.40×10^{43}
FRB20181218A	600	1874.41	147.21	1727.20	0.83	1.44	10.64	5.01×10^{43}
FRB20181218B	600	753.41	169.61	583.80	0.56	0.49	2.82	2.81×10^{42}
FRB20181218C	600	384.15	64.35	319.80	0.25	0.27	1.40	3.24×10^{41}
FRB20181219B	600	1952.17	37.27	1914.90	4.60	1.60	12.08	3.51×10^{44}
FRB20181219C	600	647.89	36.19	611.70	0.21	0.51	2.99	1.16×10^{42}
FRB20181220A	600	209.40	125.80	83.60	1.33	0.07	0.32	9.83×10^{40}
FRB20181220B	600	257.80	53.60	204.20	2.90	0.17	0.85	1.41×10^{42}
FRB20181221A	600	316.24	24.44	291.80	1.25	0.24	1.26	1.32×10^{42}
FRB20181221B	600	1395.02	61.92	1333.10	0.97	1.11	7.73	3.25×10^{43}
FRB20181222B	600	619.25	148.25	471.00	0.46	0.39	2.19	1.42×10^{42}
FRB20181222C	600	1104.89	46.39	1058.50	0.84	0.88	5.82	1.65×10^{43}
FRB20181222D	600	1417.11	31.21	1385.90	0.22	1.15	8.11	8.05×10^{42}
FRB20181222E	600	327.98	59.88	268.10	1.12	0.22	1.15	9.86×10^{41}
FRB20181223B	600	565.66	25.45	540.20	0.68	0.45	2.57	2.86×10^{42}
FRB20181223C	600	112.51	19.91	92.60	1.36	0.08	0.36	1.24×10^{41}
FRB20181224A	600	310.21	85.01	225.20	4.30	0.19	0.94	2.59×10^{42}
FRB20181224B	600	781.01	121.31	659.70	0.77	0.55	3.27	5.11×10^{42}
FRB20181224C	600	596.33	55.33	541.00	0.50	0.45	2.58	2.11×10^{42}
FRB20181224D	600	690.20	31.40	658.80	0.54	0.55	3.27	3.57×10^{42}
FRB20181224E	600	581.85	36.55	545.30	3.60	0.45	2.60	1.55×10^{43}
FRB20181225B	600	299.29	58.29	241.00	1.90	0.20	1.02	1.33×10^{42}
FRB20181226B	600	287.04	27.74	259.30	8.90	0.22	1.10	7.28×10^{42}
FRB20181226C	600	409.02	94.02	315.00	0.88	0.26	1.37	1.10×10^{42}
FRB20181226D	600	385.38	64.98	320.40	1.89	0.27	1.40	2.46×10^{42}
FRB20181226E	600	308.76	68.86	239.90	0.48	0.20	1.01	3.31×10^{41}
FRB20181227A	600	791.21	89.01	702.20	0.93	0.59	3.53	7.12×10^{42}
FRB20181228A	600	748.68	34.18	714.50	1.16	0.60	3.60	9.24×10^{42}
FRB20181228B	600	568.65	39.95	528.70	0.40	0.44	2.51	1.60×10^{42}
FRB20181228C	600	510.70	45.60	465.10	0.45	0.39	2.16	1.35×10^{42}
FRB20181229A	600	955.57	42.97	912.60	1.18	0.76	4.85	1.65×10^{43}
FRB20181229B	600	389.05	29.35	359.70	0.42	0.30	1.60	7.07×10^{41}
FRB20181230A	600	769.61	68.41	701.20	0.94	0.58	3.52	7.17×10^{42}
FRB20181230B	600	1137.36	84.96	1052.40	0.88	0.88	5.78	1.71×10^{43}
FRB20181230C	600	1037.19	36.89	1000.30	0.89	0.83	5.43	1.54×10^{43}
FRB20181230D	600	223.97	40.57	183.40	1.39	0.15	0.75	5.37×10^{41}
FRB20181230E	600	1041.71	54.51	987.20	1.32	0.82	5.34	2.21×10^{43}
FRB20181231A	600	1376.73	43.03	1333.70	1.09	1.11	7.74	3.65×10^{43}
FRB20181231B	600	197.17	46.87	150.30	0.89	0.13	0.61	2.25×10^{41}
FRB20181231C	600	556.09	35.49	520.60	0.68	0.43	2.46	2.63×10^{42}
FRB20190101A	600	854.61	24.31	830.30	0.60	0.69	4.32	6.75×10^{42}
FRB20190101B	600	1323.91	234.01	1089.90	1.02	0.91	6.03	2.15×10^{43}
FRB20190102A	600	699.17	43.57	655.60	1.12	0.55	3.25	7.33×10^{42}
FRB20190102B	600	367.16	41.06	326.10	1.71	0.27	1.43	2.32×10^{42}
FRB20190103B	600	541.13	187.13	354.00	0.68	0.30	1.57	1.10×10^{42}
FRB20190103C	600	1349.13	155.53	1193.60	2.30	0.99	6.75	5.97×10^{43}
FRB20190103D	600	1913.55	33.25	1880.30	0.45	1.57	11.82	3.29×10^{43}

Table A1. *Cont.*

TNS Name	ν_c (MHz)	DM (pc cm^{-3})	DM_{MW} (pc cm^{-3})	DM_{E} (pc cm^{-3})	S_{peak} (Jy ms)	z	D_{L} (Gpc)	L_{p} (erg s^{-1})
FRB20190103E	600	736.25	45.65	690.60	0.46	0.58	3.46	3.39×10^{42}
FRB20190104A	600	549.43	151.53	397.90	1.45	0.33	1.80	3.06×10^{42}
FRB20190104B	600	530.14	49.84	480.30	2.70	0.40	2.24	8.70×10^{42}
FRB20190105A	600	383.55	46.35	337.20	0.60	0.28	1.49	8.75×10^{41}
FRB20190106A	600	340.06	88.86	251.20	0.27	0.21	1.06	2.06×10^{41}
FRB20190106B	600	316.59	141.69	174.90	1.70	0.15	0.71	5.94×10^{41}
FRB20190107A	600	849.19	39.89	809.30	0.49	0.67	4.19	5.20×10^{42}
FRB20190107B	600	166.09	69.99	96.10	2.80	0.08	0.38	2.76×10^{41}
FRB20190109A	600	324.60	147.70	176.90	1.19	0.15	0.72	4.26×10^{41}
FRB20190109B	600	175.17	68.27	106.90	1.20	0.09	0.42	1.48×10^{41}
FRB20190110A	600	472.75	188.55	284.20	1.54	0.24	1.22	1.54×10^{42}
FRB20190110B	600	486.12	45.52	440.60	0.47	0.37	2.02	1.25×10^{42}
FRB20190110C	600	221.96	35.66	186.30	0.64	0.16	0.76	2.56×10^{41}
FRB20190111A	600	171.97	21.47	150.50	3.60	0.13	0.61	9.13×10^{41}
FRB20190111B	600	1336.93	65.13	1271.80	0.32	1.06	7.30	9.61×10^{42}
FRB20190112A	600	425.85	42.05	383.80	1.40	0.32	1.72	2.72×10^{42}
FRB20190113A	600	428.92	178.92	250.00	1.30	0.21	1.06	9.82×10^{41}
FRB20190114A	600	887.39	38.09	849.30	0.55	0.71	4.44	6.52×10^{42}
FRB20190115A	600	1021.68	186.38	835.30	0.46	0.70	4.35	5.25×10^{42}
FRB20190115B	600	748.29	63.79	684.50	1.45	0.57	3.42	1.05×10^{43}
FRB20190116C	600	629.28	41.88	587.40	28.00	0.49	2.85	1.42×10^{44}
FRB20190116D	600	1164.03	78.53	1085.50	0.51	0.90	6.00	1.06×10^{43}
FRB20190116E	600	1491.00	128.40	1362.60	0.46	1.14	7.95	1.62×10^{43}
FRB20190116F	600	316.92	46.82	270.10	0.49	0.23	1.15	4.38×10^{41}
FRB20190117C	600	865.90	53.30	812.60	0.42	0.68	4.21	4.50×10^{42}
FRB20190117D	600	1178.06	22.56	1155.50	0.78	0.96	6.48	1.88×10^{43}
FRB20190118A	600	225.11	53.41	171.70	9.30	0.14	0.70	3.12×10^{42}
FRB20190118B	600	670.89	50.19	620.70	0.31	0.52	3.04	1.79×10^{42}
FRB20190121A	600	425.35	87.35	338.00	1.70	0.28	1.49	2.49×10^{42}
FRB20190122A	600	1231.21	64.61	1166.60	0.33	0.97	6.56	8.06×10^{42}
FRB20190122B	600	469.57	54.47	415.10	0.41	0.35	1.89	9.51×10^{41}
FRB20190122C	600	689.90	24.40	665.50	4.20	0.55	3.31	2.84×10^{43}
FRB20190124A	600	1275.85	176.55	1099.30	0.61	0.92	6.10	1.31×10^{43}
FRB20190124B	600	441.38	21.58	419.80	0.97	0.35	1.91	2.31×10^{42}
FRB20190124C	600	303.64	21.44	282.20	2.50	0.24	1.21	2.46×10^{42}
FRB20190124D	600	340.12	45.62	294.50	0.50	0.25	1.27	5.41×10^{41}
FRB20190124E	600	617.79	391.99	225.80	0.64	0.19	0.95	3.87×10^{41}
FRB20190124F	600	254.79	37.59	217.20	3.90	0.18	0.91	2.17×10^{42}
FRB20190125A	600	564.70	60.40	504.30	0.37	0.42	2.37	1.33×10^{42}
FRB20190125B	600	178.24	33.24	145.00	0.83	0.12	0.58	1.94×10^{41}
FRB20190127B	600	663.03	48.43	614.60	0.63	0.51	3.00	3.56×10^{42}
FRB20190128A	600	696.12	43.62	652.50	0.58	0.54	3.23	3.75×10^{42}
FRB20190128B	600	248.23	57.23	191.00	0.81	0.16	0.79	3.42×10^{41}
FRB20190128C	600	310.62	71.32	239.30	0.71	0.20	1.01	4.88×10^{41}
FRB20190128D	600	430.23	232.83	197.40	1.20	0.16	0.81	5.43×10^{41}
FRB20190129A	600	484.76	52.06	432.70	0.49	0.36	1.98	1.25×10^{42}
FRB20190130A	600	1367.46	37.36	1330.10	0.47	1.11	7.71	1.56×10^{43}
FRB20190130B	600	989.03	29.73	959.30	0.77	0.80	5.16	1.21×10^{43}
FRB20190131B	600	1805.73	35.63	1770.10	0.99	1.48	10.97	6.32×10^{43}
FRB20190131C	600	507.76	32.96	474.80	0.84	0.40	2.21	2.64×10^{42}
FRB20190131D	600	642.12	67.52	574.60	2.90	0.48	2.77	1.40×10^{43}
FRB20190131E	600	279.80	43.30	236.50	3.00	0.20	1.00	2.01×10^{42}
FRB20190201A	600	242.00	62.40	179.60	2.60	0.15	0.73	9.61×10^{41}
FRB20190201B	600	749.18	54.18	695.00	0.81	0.58	3.48	6.06×10^{42}

Table A1. *Cont.*

TNS Name	ν_c (MHz)	DM (pc cm^{-3})	$DM_{\rm MW}$ (pc cm^{-3})	$DM_{\rm E}$ (pc cm^{-3})	$S_{\rm peak}$ (Jy ms)	z	$D_{\rm L}$ (Gpc)	$L_{\rm p}$ (erg s^{-1})
FRB20190202A	600	307.36	40.76	266.60	41.00	0.22	1.14	3.56×10^{43}
FRB20190202B	600	464.91	70.11	394.80	1.57	0.33	1.78	3.25×10^{42}
FRB20190203A	600	420.57	45.87	374.70	1.21	0.31	1.68	2.23×10^{42}
FRB20190203B	600	582.22	45.82	536.40	0.49	0.45	2.55	2.03×10^{42}
FRB20190203C	600	370.46	29.66	340.80	1.40	0.28	1.50	2.09×10^{42}
FRB20190204A	600	449.64	36.14	413.50	0.24	0.34	1.88	5.52×10^{41}
FRB20190204B	600	1464.94	45.54	1419.40	1.35	1.18	8.36	5.22×10^{43}
FRB20190205A	600	695.39	67.69	627.70	0.74	0.52	3.08	4.38×10^{42}
FRB20190206A	600	188.34	41.44	146.90	1.40	0.12	0.59	3.37×10^{41}
FRB20190206B	600	352.52	78.52	274.00	0.95	0.23	1.17	8.77×10^{41}
FRB20190206C	600	1043.00	38.30	1004.70	0.56	0.84	5.46	9.78×10^{42}
FRB20190208B	600	714.22	60.62	653.60	10.30	0.54	3.23	6.69×10^{43}
FRB20190208C	600	238.39	49.69	188.70	1.27	0.16	0.78	5.22×10^{41}
FRB20190210B	600	624.19	116.49	507.70	2.60	0.42	2.39	9.50×10^{42}
FRB20190210C	600	643.37	55.27	588.10	2.37	0.49	2.85	1.21×10^{43}
FRB20190210D	600	359.15	141.25	217.90	1.37	0.18	0.91	7.68×10^{41}
FRB20190210E	600	580.58	57.88	522.70	0.69	0.44	2.48	2.69×10^{42}
FRB20190211A	600	1188.26	103.86	1084.40	1.47	0.90	6.00	3.06×10^{43}
FRB20190211B	600	260.70	84.50	176.20	0.30	0.15	0.72	1.06×10^{41}
FRB20190212B	600	600.19	41.19	559.00	1.55	0.47	2.68	7.05×10^{42}
FRB20190212C	600	1016.45	22.35	994.10	0.70	0.83	5.39	1.19×10^{43}
FRB20190212D	600	1139.77	35.37	1104.40	0.42	0.92	6.13	9.12×10^{42}
FRB20190213C	600	357.06	175.96	181.10	0.62	0.15	0.74	2.33×10^{41}
FRB20190213D	600	1346.85	234.55	1112.30	1.00	0.93	6.19	2.21×10^{43}
FRB20190214A	600	497.68	69.78	427.90	0.46	0.36	1.96	1.14×10^{42}
FRB20190214C	600	533.11	22.11	511.00	1.02	0.43	2.41	3.78×10^{42}
FRB20190215B	600	274.63	136.23	138.40	2.20	0.12	0.55	4.67×10^{41}
FRB20190217A	600	798.11	110.71	687.40	0.29	0.57	3.44	2.11×10^{42}
FRB20190217B	600	846.21	45.81	800.40	0.54	0.67	4.13	5.59×10^{42}
FRB20190218A	600	1285.13	31.43	1253.70	0.54	1.04	7.17	1.57×10^{43}
FRB20190218B	600	547.87	81.57	466.30	0.57	0.39	2.16	1.72×10^{42}
FRB20190218C	600	319.32	43.72	275.60	19.00	0.23	1.18	1.78×10^{43}
FRB20190219A	600	657.19	78.79	578.40	0.31	0.48	2.79	1.50×10^{42}
FRB20190219B	600	1681.11	37.71	1643.40	1.10	1.37	10.01	5.94×10^{43}
FRB20190219C	600	806.69	124.09	682.60	0.40	0.57	3.41	2.87×10^{42}
FRB20190220A	600	216.12	40.92	175.20	0.34	0.15	0.71	1.19×10^{41}
FRB20190221A	600	223.81	52.91	170.90	1.23	0.14	0.70	4.09×10^{41}
FRB20190221B	600	393.12	165.52	227.60	0.69	0.19	0.95	4.25×10^{41}
FRB20190221C	600	2042.30	220.60	1821.70	0.59	1.52	11.37	4.02×10^{43}
FRB20190221D	600	473.79	189.59	284.20	0.65	0.24	1.22	6.50×10^{41}
FRB20190222B	600	497.62	33.22	464.40	0.40	0.39	2.15	1.19×10^{42}
FRB20190222C	600	524.01	29.51	494.50	0.44	0.41	2.32	1.51×10^{42}
FRB20190222D	600	895.30	115.60	779.70	0.79	0.65	4.00	7.69×10^{42}
FRB20190223A	600	389.24	58.14	331.10	0.47	0.28	1.45	6.58×10^{41}
FRB20190223B	600	536.51	124.71	411.80	0.55	0.34	1.87	1.25×10^{42}
FRB20190224A	600	818.40	65.50	752.90	0.63	0.63	3.84	5.66×10^{42}
FRB20190224B	600	839.37	51.37	788.00	2.00	0.66	4.06	2.00×10^{43}
FRB20190224C	600	497.40	59.90	437.50	1.37	0.36	2.01	3.58×10^{42}
FRB20190224D	600	752.95	56.25	696.70	2.75	0.58	3.49	2.07×10^{43}
FRB20190224E	600	435.86	33.06	402.80	2.03	0.34	1.82	4.40×10^{42}
FRB20190226A	600	601.57	91.27	510.30	1.45	0.43	2.41	5.36×10^{42}
FRB20190226B	600	631.60	50.70	580.90	0.38	0.48	2.81	1.89×10^{42}
FRB20190226C	600	827.77	44.47	783.30	0.39	0.65	4.03	3.84×10^{42}
FRB20190227A	600	394.04	63.44	330.60	3.58	0.28	1.45	5.00×10^{42}

Table A1. *Cont.*

TNS Name	ν_c (MHz)	DM (pc cm^{-3})	$DM_{\rm MW}$ (pc cm^{-3})	$DM_{\rm E}$ (pc cm^{-3})	$S_{\rm peak}$ (Jy ms)	z	$D_{\rm L}$ (Gpc)	$L_{\rm p}$ (erg s^{-1})
FRB20190227B	600	331.23	23.93	307.30	0.48	0.26	1.34	5.70×10^{41}
FRB20190228A	600	419.08	20.18	398.90	1.79	0.33	1.80	3.80×10^{42}
FRB20190228B	600	1115.25	71.35	1043.90	4.80	0.87	5.72	9.16×10^{43}
FRB20190301B	600	621.33	82.83	538.50	0.40	0.45	2.57	1.67×10^{42}
FRB20190301C	600	802.91	20.51	782.40	0.34	0.65	4.02	3.34×10^{42}
FRB20190301D	600	1160.69	53.09	1107.60	0.39	0.92	6.15	8.53×10^{42}
FRB20190302A	600	1034.24	220.74	813.50	0.56	0.68	4.22	6.01×10^{42}
FRB20190303B	600	193.51	47.11	146.40	9.40	0.12	0.59	2.25×10^{42}
FRB20190303C	600	1089.66	23.06	1066.60	0.80	0.89	5.87	1.60×10^{43}
FRB20190303D	600	711.15	37.05	674.10	0.59	0.56	3.36	4.11×10^{42}
FRB20190304A	600	483.73	49.83	433.90	0.71	0.36	1.99	1.82×10^{42}
FRB20190304B	600	470.01	22.61	447.40	0.67	0.37	2.06	1.84×10^{42}
FRB20190304C	600	564.99	22.09	542.90	0.53	0.45	2.59	2.25×10^{42}
FRB20190307A	600	355.34	58.04	297.30	…	0.25	1.29	…
FRB20190307B	600	294.00	54.90	239.10	…	0.20	1.01	…
FRB20190308B	600	180.18	68.68	111.50	1.11	0.09	0.44	1.49×10^{41}
FRB20190308C	600	500.52	23.12	477.40	0.47	0.40	2.22	1.49×10^{42}
FRB20190309A	600	356.90	58.60	298.30	0.39	0.25	1.29	4.34×10^{41}
FRB20190313B	600	1191.25	59.85	1131.40	0.67	0.94	6.32	1.54×10^{43}
FRB20190316A	600	515.93	38.93	477.00	1.31	0.40	2.22	4.16×10^{42}
FRB20190317A	600	1157.26	137.96	1019.30	0.54	0.85	5.56	9.75×10^{42}
FRB20190317B	600	424.31	80.61	343.70	0.65	0.29	1.52	9.89×10^{41}
FRB20190317C	600	598.26	53.56	544.70	0.43	0.45	2.60	1.84×10^{42}
FRB20190317E	600	800.88	134.28	666.60	2.17	0.56	3.31	1.47×10^{43}
FRB20190317F	600	1118.11	33.31	1084.80	1.65	0.90	6.00	3.44×10^{43}
FRB20190318A	600	419.27	85.37	333.90	1.55	0.28	1.47	2.21×10^{42}
FRB20190319A	600	2039.94	107.64	1932.30	2.78	1.61	12.22	2.16×10^{44}
FRB20190320A	600	614.15	143.95	470.20	0.94	0.39	2.19	2.89×10^{42}
FRB20190320B	600	489.49	37.69	451.80	0.73	0.38	2.09	2.05×10^{42}
FRB20190320C	600	368.79	47.09	321.70	1.24	0.27	1.41	1.63×10^{42}
FRB20190320D	600	1141.35	43.85	1097.50	0.49	0.91	6.08	1.05×10^{43}
FRB20190320E	600	299.14	55.84	243.30	4.40	0.20	1.03	3.13×10^{42}
FRB20190322A	600	1060.12	63.62	996.50	0.64	0.83	5.40	1.10×10^{43}
FRB20190322B	600	576.98	46.98	530.00	0.61	0.44	2.52	2.46×10^{42}
FRB20190322C	600	1192.08	65.78	1126.30	4.10	0.94	6.28	9.32×10^{43}
FRB20190323A	600	857.50	72.80	784.70	0.67	0.65	4.04	6.62×10^{42}
FRB20190323B	600	789.56	40.26	749.30	6.94	0.62	3.81	6.17×10^{43}
FRB20190323C	600	381.12	23.62	357.50	0.56	0.30	1.59	9.30×10^{41}
FRB20190323D	600	763.65	162.35	601.30	0.37	0.50	2.93	1.99×10^{42}
FRB20190325A	600	359.29	50.99	308.30	1.31	0.26	1.34	1.57×10^{42}
FRB20190325B	600	1733.92	19.82	1714.10	0.70	1.43	10.54	4.16×10^{43}
FRB20190325C	600	797.83	188.43	609.40	0.63	0.51	2.97	3.49×10^{42}
FRB20190326A	600	283.31	40.71	242.60	1.02	0.20	1.02	7.22×10^{41}
FRB20190327A	600	346.57	88.77	257.80	2.43	0.21	1.10	1.96×10^{42}
FRB20190328A	600	1303.58	51.78	1251.80	0.43	1.04	7.16	1.25×10^{43}
FRB20190328B	600	565.00	50.10	514.90	0.72	0.43	2.43	2.72×10^{42}
FRB20190328C	600	472.86	64.66	408.20	4.70	0.34	1.85	1.05×10^{43}
FRB20190329A	600	188.61	87.81	100.80	0.52	0.08	0.40	5.67×10^{40}
FRB20190329B	600	406.05	65.95	340.10	…	0.28	1.50	…
FRB20190329C	600	1256.36	60.36	1196.00	…	1.00	6.76	…
FRB20190330A	600	508.97	24.87	484.10	0.37	0.40	2.26	1.21×10^{42}
FRB20190330B	600	668.09	48.89	619.20	2.79	0.52	3.03	1.60×10^{43}
FRB20190401A	600	783.22	42.42	740.80	1.05	0.62	3.76	9.09×10^{42}
FRB20190402A	600	1291.69	26.39	1265.30	0.30	1.05	7.25	8.91×10^{42}

Table A1. *Cont.*

TNS Name	ν_c (MHz)	DM (pc cm^{-3})	$DM_{\rm MW}$ (pc cm^{-3})	$DM_{\rm E}$ (pc cm^{-3})	$S_{\rm peak}$ (Jy ms)	z	$D_{\rm L}$ (Gpc)	$L_{\rm p}$ (erg s^{-1})
FRB20190403A	600	518.83	54.23	464.60	1.12	0.39	2.15	3.35×10^{42}
FRB20190403B	600	292.47	54.07	238.40	2.70	0.20	1.00	1.84×10^{42}
FRB20190403C	600	935.01	38.91	896.10	0.37	0.75	4.74	4.96×10^{42}
FRB20190403D	600	613.46	62.96	550.50	0.65	0.46	2.63	2.85×10^{42}
FRB20190403E	600	226.20	49.90	176.30	3.90	0.15	0.72	1.39×10^{42}
FRB20190403F	600	664.18	67.38	596.80	0.58	0.50	2.90	3.06×10^{42}
FRB20190403G	600	865.31	165.31	700.00	0.75	0.58	3.51	5.70×10^{42}
FRB20190404A	600	1353.90	40.30	1313.60	1.17	1.09	7.59	3.79×10^{43}
FRB20190404B	600	489.42	45.02	444.40	8.60	0.37	2.05	2.33×10^{43}
FRB20190405A	600	424.88	47.28	377.60	0.65	0.31	1.69	1.22×10^{42}
FRB20190405B	600	1113.22	53.92	1059.30	3.40	0.88	5.83	6.71×10^{43}
FRB20190408A	600	863.38	45.98	817.40	0.64	0.68	4.24	6.95×10^{42}
FRB20190409A	600	1791.89	84.39	1707.50	3.00	1.42	10.49	1.77×10^{44}
FRB20190409B	600	285.63	47.83	237.80	0.39	0.20	1.00	2.64×10^{41}
FRB20190409C	600	674.63	43.03	631.60	1.04	0.53	3.10	6.25×10^{42}
FRB20190409D	600	1300.12	54.72	1245.40	0.59	1.04	7.11	1.69×10^{43}
FRB20190410A	600	284.02	128.52	155.50	1.59	0.13	0.63	4.32×10^{41}
FRB20190410B	600	642.17	78.37	563.80	0.22	0.47	2.71	1.02×10^{42}
FRB20190411A	600	460.56	60.76	399.80	1.24	0.33	1.81	2.64×10^{42}
FRB20190411B	600	1229.58	35.28	1194.30	0.89	1.00	6.75	2.31×10^{43}
FRB20190411C	600	233.66	38.86	194.80	3.19	0.16	0.80	1.40×10^{42}
FRB20190412A	600	364.73	37.53	327.20	1.77	0.27	1.44	2.42×10^{42}
FRB20190412B	600	375.75	264.85	110.90	0.68	0.09	0.44	9.06×10^{40}
FRB20190414A	600	811.98	20.18	791.80	0.44	0.66	4.08	4.44×10^{42}
FRB20190414B	600	506.49	37.79	468.70	0.49	0.39	2.18	1.49×10^{42}
FRB20190415A	600	633.68	36.98	596.70	0.57	0.50	2.90	3.01×10^{42}
FRB20190415B	600	722.99	155.39	567.60	0.85	0.47	2.73	4.00×10^{42}
FRB20190415C	600	650.18	168.48	481.70	0.46	0.40	2.25	1.49×10^{42}
FRB20190416A	600	2287.27	39.17	2248.10	0.60	1.87	14.71	6.56×10^{43}
FRB20190416B	600	575.36	20.56	554.80	0.69	0.46	2.66	3.08×10^{42}
FRB20190417B	600	1161.20	35.00	1126.20	0.46	0.94	6.28	1.04×10^{43}
FRB20190417C	600	320.23	122.03	198.20	7.90	0.17	0.82	3.61×10^{42}
FRB20190418A	600	184.51	70.11	114.40	0.99	0.10	0.45	1.41×10^{41}
FRB20190419A	600	439.97	62.27	377.70	0.41	0.31	1.69	7.70×10^{41}
FRB20190419B	600	165.08	52.28	112.80	4.60	0.09	0.45	6.35×10^{41}
FRB20190420A	600	609.10	65.70	543.40	0.88	0.45	2.59	3.75×10^{42}
FRB20190420B	600	846.84	67.44	779.40	2.20	0.65	4.00	2.14×10^{43}
FRB20190420C	600	629.95	35.75	594.20	0.44	0.50	2.88	2.30×10^{42}
FRB20190421B	600	392.25	96.45	295.80	5.10	0.25	1.28	5.57×10^{42}
FRB20190422A	600	452.30	79.50	372.80	0.60	0.31	1.67	1.09×10^{42}
FRB20190422B	600	977.39	34.09	943.30	0.22	0.79	5.05	3.32×10^{42}
FRB20190423A	600	242.65	31.65	211.00	10.80	0.18	0.88	5.65×10^{42}
FRB20190423B	600	584.95	482.65	102.30	0.87	0.09	0.40	9.78×10^{40}
FRB20190423C	600	855.53	60.43	795.10	1.23	0.66	4.10	1.25×10^{43}
FRB20190423D	600	496.46	66.16	430.30	1.71	0.36	1.97	4.30×10^{42}
FRB20190424A	600	758.67	35.47	723.20	1.13	0.60	3.65	9.26×10^{42}
FRB20190425A	600	128.16	48.76	79.40	18.60	0.07	0.31	1.23×10^{42}
FRB20190425B	600	1031.72	52.72	979.00	1.25	0.82	5.29	2.06×10^{43}
FRB20190426A	600	340.66	55.86	284.80	1.59	0.24	1.23	1.60×10^{42}
FRB20190427A	600	455.78	84.98	370.80	3.90	0.31	1.66	7.03×10^{42}
FRB20190428A	600	969.40	27.00	942.40	2.22	0.79	5.05	3.35×10^{43}
FRB20190429A	600	470.88	57.58	413.30	0.80	0.34	1.88	1.84×10^{42}
FRB20190429B	600	295.65	42.15	253.50	0.74	0.21	1.08	5.76×10^{41}
FRB20190430A	600	339.25	57.85	281.40	0.75	0.23	1.21	7.34×10^{41}

Table A1. *Cont.*

TNS Name	ν_c (MHz)	DM (pc cm^{-3})	$DM_{\rm MW}$ (pc cm^{-3})	$DM_{\rm E}$ (pc cm^{-3})	$S_{\rm peak}$ (Jy ms)	z	$D_{\rm L}$ (Gpc)	$L_{\rm p}$ (erg s^{-1})
FRB20190430B	600	2619.40	36.40	2583.00	0.38	2.15	17.43	5.65×10^{43}
FRB20190430C	600	400.56	99.06	301.50	2.17	0.25	1.31	2.47×10^{42}
FRB20190501B	600	784.07	43.57	740.50	0.88	0.62	3.76	7.61×10^{42}
FRB20190502A	600	625.77	34.97	590.80	3.18	0.49	2.87	1.64×10^{43}
FRB20190502B	600	918.61	33.81	884.80	2.58	0.74	4.67	3.36×10^{43}
FRB20190502C	600	396.84	47.44	349.40	3.60	0.29	1.55	5.68×10^{42}
FRB20190515A	600	450.50	157.40	293.10	0.55	0.24	1.27	5.89×10^{41}
FRB20190515B	600	822.19	32.49	789.70	2.80	0.66	4.07	2.81×10^{43}
FRB20190515D	600	426.06	47.76	378.30	3.00	0.32	1.70	5.65×10^{42}
FRB20190516B	600	1235.42	33.32	1202.10	1.13	1.00	6.81	2.98×10^{43}
FRB20190517C	600	335.57	187.97	147.60	3.10	0.12	0.59	7.54×10^{41}
FRB20190517D	600	1180.15	93.35	1086.80	0.45	0.91	6.01	9.42×10^{42}
FRB20190518B	600	913.77	26.07	887.70	1.53	0.74	4.69	2.01×10^{43}
FRB20190518C	600	444.08	41.68	402.40	6.70	0.34	1.82	1.45×10^{43}
FRB20190518D	600	202.46	53.96	148.50	1.36	0.12	0.60	3.35×10^{41}
FRB20190518G	600	524.95	63.05	461.90	0.99	0.38	2.14	2.92×10^{42}
FRB20190519D	600	539.77	30.47	509.30	0.36	0.42	2.40	1.32×10^{42}
FRB20190519E	600	693.83	27.53	666.30	1.00	0.56	3.31	6.79×10^{42}
FRB20190519F	600	797.77	42.07	755.70	0.75	0.63	3.85	6.80×10^{42}
FRB20190519G	600	430.09	73.49	356.60	1.11	0.30	1.58	1.83×10^{42}
FRB20190519H	600	1170.87	59.37	1111.50	3.20	0.93	6.18	7.05×10^{43}
FRB20190519J	600	642.76	56.06	586.70	0.63	0.49	2.84	3.20×10^{42}
FRB20190520A	600	432.51	79.71	352.80	1.08	0.29	1.56	1.74×10^{42}
FRB20190527A	600	584.58	33.68	550.90	0.47	0.46	2.64	2.07×10^{42}
FRB20190527C	600	535.44	73.84	461.60	3.00	0.38	2.14	8.84×10^{42}
FRB20190529A	600	704.45	165.45	539.00	0.47	0.45	2.57	1.97×10^{42}
FRB20190530A	600	555.45	139.25	416.20	0.58	0.35	1.89	1.35×10^{42}
FRB20190531A	600	324.70	44.00	280.70	…	0.23	1.21	…
FRB20190531B	600	167.96	43.06	124.90	…	0.10	0.50	…
FRB20190531C	600	478.20	132.40	345.80	0.37	0.29	1.53	5.71×10^{41}
FRB20190531E	600	328.20	32.00	296.20	2.70	0.25	1.28	2.96×10^{42}
FRB20190601A	600	2227.89	32.99	2194.90	0.73	1.83	14.29	7.56×10^{43}
FRB20190601B	600	787.80	41.90	745.90	1.00	0.62	3.79	8.80×10^{42}
FRB20190601C	600	424.07	186.37	237.70	1.32	0.20	1.00	8.93×10^{41}
FRB20190601D	600	668.47	63.87	604.60	0.63	0.50	2.95	3.42×10^{42}
FRB20190603B	600	504.32	100.32	404.00	1.70	0.34	1.83	3.71×10^{42}
FRB20190604C	600	515.64	163.94	351.70	1.56	0.29	1.56	2.50×10^{42}
FRB20190604D	600	1021.17	24.77	996.40	0.82	0.83	5.40	1.40×10^{43}
FRB20190604E	600	1218.60	26.00	1192.60	1.16	0.99	6.74	3.01×10^{43}
FRB20190604G	600	233.05	51.45	181.60	1.15	0.15	0.74	4.35×10^{41}
FRB20190605C	600	187.64	37.84	149.80	4.60	0.12	0.60	1.15×10^{42}
FRB20190605D	600	1656.53	48.83	1607.70	0.82	1.34	9.74	4.21×10^{43}
FRB20190606B	600	277.49	55.09	222.40	2.62	0.19	0.93	1.53×10^{42}
FRB20190607A	600	562.45	43.95	518.50	4.35	0.43	2.45	1.67×10^{43}
FRB20190607B	600	289.38	138.28	151.10	1.06	0.13	0.61	2.71×10^{41}
FRB20190608A	600	722.18	38.38	683.80	1.29	0.57	3.42	9.29×10^{42}
FRB20190609A	600	316.64	58.44	258.20	3.60	0.22	1.10	2.92×10^{42}
FRB20190609B	600	292.19	52.29	239.90	11.50	0.20	1.01	7.94×10^{42}
FRB20190609C	600	480.28	112.68	367.60	0.64	0.31	1.64	1.13×10^{42}
FRB20190609D	600	511.71	57.51	454.20	0.66	0.38	2.10	1.87×10^{42}
FRB20190612A	600	432.29	41.69	390.60	0.79	0.33	1.76	1.60×10^{42}
FRB20190612B	600	187.60	27.70	159.90	2.41	0.13	0.65	6.95×10^{41}
FRB20190612C	600	1641.57	107.77	1533.80	3.80	1.28	9.19	1.75×10^{44}
FRB20190613A	600	714.98	53.48	661.50	1.07	0.55	3.28	7.14×10^{42}
FRB20190613B	600	285.14	168.84	116.30	1.08	0.10	0.46	1.59×10^{41}

Table A1. *Cont.*

TNS Name	ν_c (MHz)	DM (pc cm^{-3})	DM_{MW} (pc cm^{-3})	DM_E (pc cm^{-3})	S_{peak} (Jy ms)	z	D_L (Gpc)	L_p (erg s^{-1})
FRB20190614A	600	1064.04	52.34	1011.70	0.83	0.84	5.51	1.47×10^{43}
FRB20190614B	600	581.91	54.91	527.00	4.50	0.44	2.50	1.79×10^{43}
FRB20190614C	600	589.16	57.46	531.70	0.50	0.44	2.53	2.03×10^{42}
FRB20190616A	600	212.59	25.49	187.10	0.73	0.16	0.77	2.95×10^{41}
FRB20190617A	600	195.77	46.67	149.10	5.80	0.12	0.60	1.44×10^{42}
FRB20190617B	600	273.51	43.81	229.70	0.99	0.19	0.96	6.22×10^{41}
FRB20190617C	600	640.16	45.36	594.80	0.54	0.50	2.89	2.83×10^{42}
FRB20190618A	600	228.95	77.25	151.70	2.40	0.13	0.61	6.19×10^{41}
FRB20190619A	600	899.91	37.61	862.30	1.57	0.72	4.53	1.93×10^{43}
FRB20190619B	600	270.59	45.89	224.70	1.96	0.19	0.94	1.17×10^{42}
FRB20190619C	600	488.27	69.27	419.00	0.72	0.35	1.91	1.71×10^{42}
FRB20190619D	600	378.47	63.97	314.50	0.48	0.26	1.37	6.00×10^{41}
FRB20190621B	600	1061.23	30.73	1030.50	0.30	0.86	5.63	5.55×10^{42}
FRB20190621C	600	570.27	25.67	544.60	1.98	0.45	2.60	8.48×10^{42}
FRB20190621D	600	647.51	50.71	596.80	0.89	0.50	2.90	4.70×10^{42}
FRB20190622A	600	1122.82	56.82	1066.00	0.61	0.89	5.87	1.22×10^{43}
FRB20190623A	600	1082.20	74.20	1008.00	0.41	0.84	5.48	7.21×10^{42}
FRB20190623B	600	1556.77	143.77	1413.00	1.58	1.18	8.31	6.04×10^{43}
FRB20190623C	600	1049.83	48.83	1001.00	1.92	0.83	5.43	3.32×10^{43}
FRB20190624A	600	973.85	37.85	936.00	0.58	0.78	5.00	8.60×10^{42}
FRB20190624B	600	213.92	69.72	144.20	16.50	0.12	0.58	3.82×10^{42}
FRB20190625A	600	302.14	23.14	279.00	0.35	0.23	1.20	3.36×10^{41}
FRB20190625C	600	442.24	76.14	366.10	2.22	0.31	1.63	3.89×10^{42}
FRB20190625D	600	717.88	101.38	616.50	5.30	0.51	3.01	3.01×10^{43}
FRB20190627A	600	404.22	30.32	373.90	1.98	0.31	1.67	3.63×10^{42}
FRB20190627B	600	430.32	42.02	388.30	4.06	0.32	1.75	8.11×10^{42}
FRB20190627C	600	968.61	48.01	920.60	4.00	0.77	4.90	5.71×10^{43}
FRB20190627D	600	2002.24	132.04	1870.20	0.24	1.56	11.74	1.71×10^{43}
FRB20190628A	600	745.84	29.84	716.00	0.81	0.60	3.61	6.49×10^{42}
FRB20190628B	600	408.01	46.51	361.50	0.75	0.30	1.61	1.28×10^{42}
FRB20190628C	600	1748.44	98.84	1649.60	0.38	1.37	10.06	2.07×10^{43}
FRB20190629A	600	503.78	35.08	468.70	0.82	0.39	2.18	2.50×10^{42}
FRB20190630B	600	652.15	150.55	501.60	0.92	0.42	2.36	3.27×10^{42}
FRB20190630C	600	1660.35	68.05	1592.30	0.66	1.33	9.63	3.32×10^{43}
FRB20190630D	600	323.52	43.72	279.80	1.73	0.23	1.20	1.67×10^{42}
FRB20190701A	600	637.09	54.29	582.80	1.26	0.49	2.82	6.30×10^{42}
FRB20190701B	600	749.11	61.51	687.60	1.10	0.57	3.44	8.03×10^{42}
FRB20190701C	600	974.20	58.40	915.80	0.88	0.76	4.87	1.24×10^{43}
FRB20190701D	600	933.36	55.96	877.40	1.33	0.73	4.62	1.70×10^{43}
FRB20190701E	600	890.48	42.38	848.10	0.68	0.71	4.44	8.04×10^{42}

References

1. Lorimer, D.R.; Bailes, M.; McLaughlin, M.A.; Narkevic, D.J.; Crawford, F. A Bright Millisecond Radio Burst of Extragalactic Origin. *Science* **2007**, *318*, 777. [CrossRef] [PubMed]
2. Thornton, D.; Stappers, B.; Bailes, M.; Barsdell, B.; Bates, S.; Bhat, N.D.R.; Burgay, M.; Burke-Spolaor, S.; Champion, D.J.; Coster, P.; et al. A Population of Fast Radio Bursts at Cosmological Distances. *Science* **2013**, *341*, 53–56. [CrossRef] [PubMed]
3. Cordes, J.M.; Chatterjee, S. Fast Radio Bursts: An Extragalactic Enigma. *Annu. Rev. Astron. Astrophys.* **2019**, *57*, 417–465. [CrossRef]
4. Petroff, E.; Barr, E.D.; Jameson, A.; Keane, E.F.; Bailes, M.; Kramer, M.; Morello, V.; Tabbara, D.; van Straten, W. FRBCAT: The Fast Radio Burst Catalogue. *Publ. Astron. Soc. Aust.* **2016**, *33*, e045. [CrossRef]
5. Li, X.J.; Dong, X.F.; Zhang, Z.B.; Li, D. Long and Short Fast Radio Bursts Are Different from Repeating and Nonrepeating Transients. *Astrophys. J.* **2021**, *923*, 230. [CrossRef]
6. CHIME/FRB Collaboration; Amiri, M.; Andersen, B.C.; Bandura, K.; Berger, S.; Bhardwaj, M.; Boyce, M.M.; Boyle, P.J.; Brar, C.; Breitman, D.; et al. The First CHIME/FRB Fast Radio Burst Catalog. *Astrophys. J.* **2021**, *257*, 59. [CrossRef]
7. Keane, E.F.; Petroff, E. Fast radio bursts: Search sensitivities and completeness. *Mon. Not. R. Astron. Soc.* **2015**, *447*, 2852–2856. [CrossRef]

8. Law, C.J.; Bower, G.C.; Burke-Spolaor, S.; Butler, B.; Lawrence, E.; Lazio, T.J.W.; Mattmann, C.A.; Rupen, M.; Siemion, A.; VanderWiel, S. A Millisecond Interferometric Search for Fast Radio Bursts with the Very Large Array. *Astrophys. J.* **2015**, *807*, 16. [CrossRef]
9. Champion, D.J.; Petroff, E.; Kramer, M.; Keith, M.J.; Bailes, M.; Barr, E.D.; Bates, S.D.; Bhat, N.D.R.; Burgay, M.; Burke-Spolaor, S.; et al. Five new fast radio bursts from the HTRU high-latitude survey at Parkes: First evidence for two-component bursts. *Mon. Not. R. Astron. Soc. Lett.* **2016**, *460*, L30–L34. [CrossRef]
10. Oppermann, N.; Connor, L.D.; Pen, U.L. The Euclidean distribution of fast radio bursts. *Mon. Not. R. Astron. Soc.* **2016**, *461*, 984–987. [CrossRef]
11. Rane, A.; Lorimer, D.R.; Bates, S.D.; McMann, N.; McLaughlin, M.A.; Rajwade, K. A search for rotating radio transients and fast radio bursts in the Parkes high-latitude pulsar survey. *Mon. Not. R. Astron. Soc.* **2016**, *455*, 2207–2215. [CrossRef]
12. Bhandari, S.; Keane, E.F.; Barr, E.D.; Jameson, A.; Petroff, E.; Johnston, S.; Bailes, M.; Bhat, N.D.R.; Burgay, M.; Burke-Spolaor, S.; et al. The SUrvey for Pulsars and Extragalactic Radio Bursts - II. New FRB discoveries and their follow-up. *Mon. Not. R. Astron. Soc.* **2018**, *475*, 1427–1446. [CrossRef]
13. Connor, L.; Petroff, E. On Detecting Repetition from Fast Radio Bursts. *Astrophys. J.* **2018**, *861*, L1. [CrossRef]
14. Patel, C.; Agarwal, D.; Bhardwaj, M.; Boyce, M.M.; Brazier, A.; Chatterjee, S.; Chawla, P.; Kaspi, V.M.; Lorimer, D.R.; McLaughlin, M.A.; et al. PALFA Single-pulse Pipeline: New Pulsars, Rotating Radio Transients, and a Candidate Fast Radio Burst. *Astrophys. J.* **2018**, *869*, 181. [CrossRef]
15. Shannon, R.M.; Macquart, J.P.; Bannister, K.W.; Ekers, R.D.; James, C.W.; Osłowski, S.; Qiu, H.; Sammons, M.; Hotan, A.W.; Voronkov, M.A.; et al. The dispersion-brightness relation for fast radio bursts from a wide-field survey. *Nature* **2018**, *562*, 386–390. [CrossRef]
16. Farah, W.; Flynn, C.; Bailes, M.; Jameson, A.; Bateman, T.; Campbell-Wilson, D.; Day, C.K.; Deller, A.T.; Green, A.J.; Gupta, V.; et al. Five new real-time detections of fast radio bursts with UTMOST. *Mon. Not. R. Astron. Soc.* **2019**, *488*, 2989–3002. [CrossRef]
17. Parent, E.; Chawla, P.; Kaspi, V.M.; Agazie, G.Y.; Blumer, H.; DeCesar, M.; Fiore, W.; Fonseca, E.; Hessels, J.W.T.; Kaplan, D.L.; et al. First Discovery of a Fast Radio Burst at 350 MHz by the GBNCC Survey. *Astrophys. J.* **2020**, *904*, 92. [CrossRef]
18. Li, D.; Wang, P.; Zhu, W.W.; Zhang, B.; Zhang, X.X.; Duan, R.; Zhang, Y.K.; Feng, Y.; Tang, N.Y.; Chatterjee, S.; et al. A bimodal burst energy distribution of a repeating fast radio burst source. *Nature* **2021**, *598*, 267–271. [CrossRef]
19. Xu, H.; Niu, J.R.; Chen, P.; Lee, K.J.; Zhu, W.W.; Dong, S.; Zhang, B.; Jiang, J.C.; Wang, B.J.; Xu, J.W.; et al. A fast radio burst source at a complex magnetised site in a barred galaxy. *arXiv* **2021**, arXiv:2111.11764.
20. Li, D.; Wang, P.; Qian, L.; Krco, M.; Jiang, P.; Yue, Y.; Jin, C.; Zhu, Y.; Pan, Z.; Nan, R.; et al. FAST in Space: Considerations for a Multibeam, Multipurpose Survey Using China's 500-m Aperture Spherical Radio Telescope (FAST). *IEEE Microw. Mag.* **2018**, *19*, 112–119. [CrossRef]
21. CHIME/FRB Collaboration; Andersen, B.C.; Bandura, K.M.; Bhardwaj, M.; Bij, A.; Boyce, M.M.; Boyle, P.J.; Brar, C.; Cassanelli, T.; Chawla, P.; et al. A bright millisecond-duration radio burst from a Galactic magnetar. *Nature* **2020**, *587*, 54–58. [CrossRef]
22. Bochenek, C. A Fast Radio Burst Associated with a Galactic Magnetar. In Proceedings of the American Astronomical Society Meeting Abstracts, New York, NY, USA, 11–15 January 2021; Volume 53, p. 236.05D.
23. Lin, L.; Zhang, C.F.; Wang, P.; Gao, H.; Guan, X.; Han, J.L.; Jiang, J.C.; Jiang, P.; Lee, K.J.; Li, D.; et al. No pulsed radio emission during a bursting phase of a Galactic magnetar. *Nature* **2020**, *587*, 63–65. [CrossRef] [PubMed]
24. Mereghetti, S.; Savchenko, V.; Ferrigno, C.; Götz, D.; Rigoselli, M.; Tiengo, A.; Bazzano, A.; Bozzo, E.; Coleiro, A.; Courvoisier, T.J.L.; et al. INTEGRAL Discovery of a Burst with Associated Radio Emission from the Magnetar SGR 1935+2154. *Astrophys. J.* **2020**, *898*, L29. [CrossRef]
25. Li, C.K.; Lin, L.; Xiong, S.L.; Ge, M.Y.; Li, X.B.; Li, T.P.; Lu, F.J.; Zhang, S.N.; Tuo, Y.L.; Nang, Y.; et al. HXMT identification of a non-thermal X-ray burst from SGR J1935+2154 and with FRB 200428. *Nat. Astron.* **2021**, *5*, 378–384. [CrossRef]
26. Ridnaia, A.; Svinkin, D.; Frederiks, D.; Bykov, A.; Popov, S.; Aptekar, R.; Golenetskii, S.; Lysenko, A.; Tsvetkova, A.; Ulanov, M.; et al. A peculiar hard X-ray counterpart of a Galactic fast radio burst. *Nat. Astron.* **2021**, *5*, 372–377. [CrossRef]
27. Tavani, M.; Casentini, C.; Ursi, A.; Verrecchia, F.; Addis, A.; Antonelli, L.A.; Argan, A.; Barbiellini, G.; Baroncelli, L.; Bernardi, G.; et al. An X-ray burst from a magnetar enlightening the mechanism of fast radio bursts. *Nat. Astron.* **2021**, *5*, 401–407. [CrossRef]
28. Petroff, E.; Hessels, J.W.T.; Lorimer, D.R. Fast radio bursts. *Astron. Astrophys.* **2019**, *27*, 4. [CrossRef]
29. Zhang, B. Fast Radio Burst Energetics and Detectability from High Redshifts. *Astrophys. J.* **2018**, *867*, L21. [CrossRef]
30. Ravi, V.; Catha, M.; D'Addario, L.; Djorgovski, S.G.; Hallinan, G.; Hobbs, R.; Kocz, J.; Kulkarni, S.R.; Shi, J.; Vedantham, H.K.; et al. A fast radio burst localized to a massive galaxy. *Nature* **2019**, *572*, 352–354. [CrossRef]
31. Platts, E.; Weltman, A.; Walters, A.; Tendulkar, S.P.; Gordin, J.E.B.; Kandhai, S. A living theory catalogue for fast radio bursts. *Phys. Rep.* **2019**, *821*, 1–27. [CrossRef]
32. Yamasaki, S.; Totani, T.; Kiuchi, K. Repeating and non-repeating fast radio bursts from binary neutron star mergers. *Publ. Astron. Soc. Jpn.* **2018**, *70*, 39. [CrossRef]
33. Popov, S.B.; Postnov, K.A. Millisecond extragalactic radio bursts as magnetar flares. *arXiv* **2013**, arXiv:1307.4924.
34. Metzger, B.D.; Margalit, B.; Sironi, L. Fast radio bursts as synchrotron maser emission from decelerating relativistic blast waves. *Mon. Not. R. Astron. Soc.* **2019**, *485*, 4091–4106. [CrossRef]
35. Geng, J.J.; Huang, Y.F. Fast Radio Bursts: Collisions between Neutron Stars and Asteroids/Comets. *Astrophys. J.* **2015**, *809*, 24. [CrossRef]

36. Dai, Z.G.; Wang, J.S.; Wu, X.F.; Huang, Y.F. Repeating Fast Radio Bursts from Highly Magnetized Pulsars Traveling through Asteroid Belts. *Astrophys. J.* **2016**, *829*, 27. [CrossRef]
37. Xiao, D.; Dai, Z.G. Double-peaked Pulse Profile of FRB 200428: Synchrotron Maser Emission from Magnetized Shocks Encountering a Density Jump. *Astrophys. J.* **2020**, *904*, L5. [CrossRef]
38. Geng, J.J.; Li, B.; Li, L.B.; Xiong, S.L.; Kuiper, R.; Huang, Y.F. FRB 200428: An Impact between an Asteroid and a Magnetar. *Astrophys. J.* **2020**, *898*, L55. [CrossRef]
39. Geng, J.; Li, B.; Huang, Y. Repeating fast radio bursts from collapses of the crust of a strange star. *Innovation* **2021**, *2*, 100152, [CrossRef]
40. Li, L.B.; Huang, Y.F.; Geng, J.J.; Li, B. A model of fast radio bursts: Collisions between episodic magnetic blobs. *Res. Astron. Astrophys.* **2018**, *18*, 061. [CrossRef]
41. Zhang, B. FRB 121102: A Repeatedly Combed Neutron Star by a Nearby Low-luminosity Accreting Supermassive Black Hole. *Astrophys. J.* **2018**, *854*, L21. [CrossRef]
42. Li, Q.C.; Yang, Y.P.; Wang, F.Y.; Xu, K.; Shao, Y.; Liu, Z.N.; Dai, Z.G. Periodic Activities of Repeating Fast Radio Bursts from Be/X-Ray Binary Systems. *Astrophys. J.* **2021**, *918*, L5, [CrossRef]
43. Yang, H.; Zou, Y.C. Orbit-induced Spin Precession as a Possible Origin for Periodicity in Periodically Repeating Fast Radio Bursts. *Astrophys. J.* **2020**, *893*, L31, [CrossRef]
44. Levin, Y.; Beloborodov, A.M.; Bransgrove, A. Precessing Flaring Magnetar as a Source of Repeating FRB 180916.J0158+65. *Astrophys. J. Lett.* **2020**, *895*, L30. [CrossRef]
45. Tong, H.; Wang, W.; Wang, H.G. Periodicity in fast radio bursts due to forced precession by a fallback disk. *Res. Astron. Astrophys.* **2020**, *20*, 142. [CrossRef]
46. Li, D.; Zanazzi, J.J. Emission Properties of Periodic Fast Radio Bursts from the Motion of Magnetars: Testing Dynamical Models. *Astrophys. J. Lett.* **2021**, *909*, L25. [CrossRef]
47. Sridhar, N.; Metzger, B.D.; Beniamini, P.; Margalit, B.; Renzo, M.; Sironi, L.; Kovlakas, K. Periodic Fast Radio Bursts from Luminous X-ray Binaries. *Astrophys. J.* **2021**, *917*, 13. [CrossRef]
48. Zhang, B. Unexpected emission pattern adds to the enigma of fast radio bursts. *Nature* **2020**, *582*, 344–346. [CrossRef]
49. Xu, K.; Li, Q.C.; Yang, Y.P.; Li, X.D.; Dai, Z.G.; Liu, J. Do the Periodic Activities of Repeating Fast Radio Bursts Represent the Spins of Neutron Stars? *Astrophys. J.* **2021**, *917*, 2. [CrossRef]
50. Thompson, A.R.; Clark, B.G.; Wade, C.M.; Napier, P.J. The Very Large Array. *Astrophys. J.* **1980**, *44*, 151–167. [CrossRef]
51. Bannister, K.W.; Shannon, R.M.; Macquart, J.P.; Flynn, C.; Edwards, P.G.; O'Neill, M.; Osłowski, S.; Bailes, M.; Zackay, B.; Clarke, N.; et al. The Detection of an Extremely Bright Fast Radio Burst in a Phased Array Feed Survey. *Astrophys. J. Lett.* **2017**, *841*, L12. [CrossRef]
52. CHIME/FRB Collaboration; Amiri, M.; Bandura, K.; Berger, P.; Bhardwaj, M.; Boyce, M.M.; Boyle, P.J.; Brar, C.; Burhanpurkar, M.; Chawla, P.; et al. The CHIME Fast Radio Burst Project: System Overview. *Astrophys. J.* **2018**, *863*, 48. [CrossRef]
53. Spitler, L.G.; Scholz, P.; Hessels, J.W.T.; Bogdanov, S.; Brazier, A.; Camilo, F.; Chatterjee, S.; Cordes, J.M.; Crawford, F.; Deneva, J.; et al. A repeating fast radio burst. *Nature* **2016**, *531*, 202–205. [CrossRef] [PubMed]
54. CHIME/FRB Collaboration; Amiri, M.; Bandura, K.; Bhardwaj, M.; Boubel, P.; Boyce, M.M.; Boyle, P.J.; . Brar, C.; Burhanpurkar, M.; Cassanelli, T.; et al. A second source of repeating fast radio bursts. *Nature* **2019**, *566*, 235–238. [CrossRef]
55. CHIME/FRB Collaboration; Andersen, B.C.; Bandura, K.; Bhardwaj, M.; Boubel, P.; Boyce, M.M.; Boyle, P.J.; Brar, C.; Cassanelli, T.; Chawla, P.; et al. CHIME/FRB Discovery of Eight New Repeating Fast Radio Burst Sources. *Astrophys. J.* **2019**, *885*, L24. [CrossRef]
56. Kumar, P.; Shannon, R.M.; Osłowski, S.; Qiu, H.; Bhandari, S.; Farah, W.; Flynn, C.; Kerr, M.; Lorimer, D.R.; Macquart, J.P.; et al. Faint Repetitions from a Bright Fast Radio Burst Source. *Astrophys. J.* **2019**, *887*, L30. [CrossRef]
57. Luo, R.; Wang, B.J.; Men, Y.P.; Zhang, C.F.; Jiang, J.C.; Xu, H.; Wang, W.Y.; Lee, K.J.; Han, J.L.; Zhang, B.; et al. Diverse polarization angle swings from a repeating fast radio burst source. *Nature* **2020**, *586*, 693–696. [CrossRef]
58. Zhang, Z.B.; Choi, C.S. An analysis of the durations of Swift gamma-ray bursts. *Astron. Astrophys.* **2008**, *484*, 293–297. [CrossRef]
59. Zhang, Z.B.; Zhang, C.T.; Zhao, Y.X.; Luo, J.J.; Jiang, L.Y.; Wang, X.L.; Han, X.L.; Terheide, R.K. Spectrum-energy Correlations in GRBs: Update, Reliability, and the Long/Short Dichotomy. *Publ. Astron. Soc. Pac.* **2018**, *130*, 054202. [CrossRef]
60. Zhang, Z.B.; Jiang, M.; Zhang, Y.; Zhang, K.; Li, X.J.; Zhang, Q. On the Spectral Peak Energy of Swift Gamma-Ray Bursts. *Astrophys. J.* **2020**, *902*, 40. [CrossRef]
61. Luo, R.; Lee, K.; Lorimer, D.R.; Zhang, B. On the normalized FRB luminosity function. *Mon. Not. R. Astron. Soc.* **2018**, *481*, 2320–2337. [CrossRef]
62. Caleb, M.; Stappers, B.W.; Rajwade, K.; Flynn, C. Are all fast radio bursts repeating sources? *Mon. Not. R. Astron. Soc.* **2019**, *484*, 5500–5508. [CrossRef]
63. Li, Y.; Zhang, B.; Nagamine, K.; Shi, J. The FRB 121102 Host Is Atypical among Nearby Fast Radio Bursts. *Astrophys. J.* **2019**, *884*, L26. [CrossRef]
64. Zhang, B. The physical mechanisms of fast radio bursts. *Nature* **2020**, *587*, 45–53. [CrossRef] [PubMed]
65. Ravi, V. The prevalence of repeating fast radio bursts. *Nat. Astron.* **2019**, *3*, 928–931. [CrossRef]
66. Lu, W.; Piro, A.L.; Waxman, E. Implications of Canadian Hydrogen Intensity Mapping Experiment repeating fast radio bursts. *Mon. Not. R. Astron. Soc.* **2020**, *498*, 1973–1982. [CrossRef]

67. Luo, R.; Men, Y.; Lee, K.; Wang, W.; Lorimer, D.R.; Zhang, B. On the FRB luminosity function—II. Event rate density. *Mon. Not. R. Astron. Soc.* **2020**, *494*, 665–679. [CrossRef]
68. Caleb, M.; Flynn, C.; Bailes, M.; Barr, E.D.; Hunstead, R.W.; Keane, E.F.; Ravi, V.; van Straten, W. Are the distributions of fast radio burst properties consistent with a cosmological population? *Mon. Not. R. Astron. Soc.* **2016**, *458*, 708–717. [CrossRef]
69. Niino, Y. Fast Radio Bursts' Recipes for the Distributions of Dispersion Measures, Flux Densities, and Fluences. *Astrophys. J.* **2018**, *858*, 4. [CrossRef]
70. Lu, W.; Piro, A.L. Implications from ASKAP Fast Radio Burst Statistics. *Astrophys. J.* **2019**, *883*, 40. [CrossRef]
71. Zhang, G.Q.; Wang, F.Y. Energy function, formation rate, and low-metallicity environment of fast radio bursts. *Mon. Not. R. Astron. Soc.* **2019**, *487*, 3672–3678. [CrossRef]
72. Bhattacharya, M.; Kumar, P. Population Modeling of Fast Radio Bursts from Source Properties. *Astrophys. J.* **2020**, *899*, 124. [CrossRef]
73. Planck Collaboration; Ade, P.A.R.; Aghanim, N.; Arnaud, M.; Ashdown, M.; Aumont, J.; Baccigalupi, C.; Banday, A.J.; Barreiro, R.B.; Bartlett, J.G.; et al. Planck 2015 results. XIII. Cosmological parameters. *Astron. Astrophys.* **2016**, *594*, A13. [CrossRef]
74. Fonseca, E.; Andersen, B.C.; Bhardwaj, M.; Chawla, P.; Good, D.C.; Josephy, A.; Kaspi, V.M.; Masui, K.W.; Mckinven, R.; Michilli, D.; et al. Nine New Repeating Fast Radio Burst Sources from CHIME/FRB. *Astrophys. J.* **2020**, *891*, L6. [CrossRef]
75. Kirsten, F.; Snelders, M.P.; Jenkins, M.; Nimmo, K.; van den Eijnden, J.; Hessels, J.W.T.; Gawroński, M.P.; Yang, J. Detection of two bright radio bursts from magnetar SGR 1935 + 2154. *Nat. Astron.* **2021**, *5*, 414–422. [CrossRef]
76. Bauer, D.F. Constructing confidence sets using rank statistics. *J. Am. Stat. Assoc.* **1972**, *67*, 687–690. [CrossRef]
77. Hollander, M.; Wolfe, D.A.; Chicken, E. *Nonparametric Statistical Methods*; John Wiley & Sons: Hoboken, NJ, USA, 2013; Volume 751.
78. Xiao, D.; Wang, F.; Dai, Z. The physics of fast radio bursts. *Sci. China Phys. Mech. Astron.* **2021**, *64*, 249501. [CrossRef]
79. Thode, H.C. *Testing for Normality*, 1st ed.; CRC Press: Boca Raton, CA, USA, 2002.
80. Li, L.B.; Huang, Y.F.; Zhang, Z.B.; Li, D.; Li, B. Intensity distribution function and statistical properties of fast radio bursts. *Res. Astron. Astrophys.* **2017**, *17*, 6. [CrossRef]
81. Nan, R.; Li, D. The five-hundred-meter aperture spherical radio telescope (FAST) project. *IOP Conf. Ser. Mater. Sci. Eng.* **2013**, *44*, 012022. [CrossRef]
82. Li, D.; Nan, R.; Pan, Z. The Five-hundred-meter Aperture Spherical radio Telescope project and its early science opportunities. In Proceedings of the Neutron Stars and Pulsars: Challenges and Opportunities after 80 Years, Beijing, China, 20–24 August 2012; van Leeuwen, J., Ed.; Cambridge University Press: Cambridge, UK, 2013; Volume 291, pp. 325–330 [CrossRef]
83. Zhang, Z.B.; Kong, S.W.; Huang, Y.F.; Li, D.; Li, L.B. Detecting radio afterglows of gamma-ray bursts with FAST. *Res. Astron. Astrophys.* **2015**, *15*, 237–251. [CrossRef]
84. Spitler, L.G.; Cordes, J.M.; Hessels, J.W.T.; Lorimer, D.R.; McLaughlin, M.A.; Chatterjee, S.; Crawford, F.; Deneva, J.S.; Kaspi, V.M.; Wharton, R.S.; et al. Fast Radio Burst Discovered in the Arecibo Pulsar ALFA Survey. *Astrophys. J.* **2014**, *790*, 101. [CrossRef]
85. Crawford, F.; Rane, A.; Tran, L.; Rolph, K.; Lorimer, D.R.; Ridley, J.P. A search for highly dispersed fast radio bursts in three Parkes multibeam surveys. *Mon. Not. R. Astron. Soc.* **2016**, *460*, 3370–3375. [CrossRef]
86. Lawrence, E.; Vander Wiel, S.; Law, C.; Burke Spolaor, S.; Bower, G.C. The Nonhomogeneous Poisson Process for Fast Radio Burst Rates. *Astron. J.* **2017**, *154*, 117. [CrossRef]
87. Bera, A.; Bhattacharyya, S.; Bharadwaj, S.; Bhat, N.D.R.; Chengalur, J.N. On modelling the Fast Radio Burst population and event rate predictions. *Mon. Not. R. Astron. Soc.* **2016**, *457*, 2530–2539. [CrossRef]
88. Aggarwal, K. Observational Effects of Banded Repeating FRBs. *Astrophys. J.* **2021**, *920*, L18, [CrossRef]
89. Zhang, Z.B.; Chandra, P.; Huang, Y.F.; Li, D. The Redshift Dependence of the Radio Flux of Gamma-Ray Bursts and Their Host Galaxies. *Astrophys. J.* **2018**, *865*, 82. [CrossRef]
90. Macquart, J.P.; Ekers, R. FRB event rate counts - II. Fluence, redshift, and dispersion measure distributions. *Mon. Not. R. Astron. Soc.* **2018**, *480*, 4211–4230. [CrossRef]
91. Macquart, J.P.; Shannon, R.M.; Bannister, K.W.; James, C.W.; Ekers, R.D.; Bunton, J.D. The Spectral Properties of the Bright Fast Radio Burst Population. *Astrophys. J.* **2019**, *872*, L19. [CrossRef]
92. Salvaterra, R.; Campana, S.; Vergani, S.D.; Covino, S.; D'Avanzo, P.; Fugazza, D.; Ghirlanda, G.; Ghisellini, G.; Melandri, A.; Nava, L.; et al. A Complete Sample of Bright Swift Long Gamma-Ray Bursts. I. Sample Presentation, Luminosity Function and Evolution. *Astrophys. J.* **2012**, *749*, 68. [CrossRef]
93. Pescalli, A.; Ghirlanda, G.; Salvaterra, R.; Ghisellini, G.; Vergani, S.; Nappo, F.; Salafia, O.; Melandri, A.; Götz, D. The rate and luminosity function of long Gamma Ray Bursts. *Astron. Astrophys.* **2015**, *587*. [CrossRef]
94. Deng, C.M.; Wang, X.G.; Guo, B.B.; Lu, R.J.; Wang, Y.Z.; Wei, J.J.; Wu, X.F.; Liang, E.W. Cosmic Evolution of Long Gamma-Ray Burst Luminosity. *Astrophys. J.* **2016**, *820*, 66. [CrossRef]
95. Gehrels, N. Confidence Limits for Small Numbers of Events in Astrophysical Data. *Astrophys. J.* **1986**, *303*, 336. . [CrossRef]
96. James, C.W.; Ekers, R.D.; Macquart, J.P.; Bannister, K.W.; Shannon, R.M. The slope of the source-count distribution for fast radio bursts. *Mon. Not. R. Astron. Soc.* **2019**, *483*, 1342–1353. [CrossRef]
97. Heintz, K.E.; Prochaska, J.X.; Simha, S.; Platts, E.; Fong, W.f.; Tejos, N.; Ryder, S.D.; Aggerwal, K.; Bhandari, S.; Day, C.K.; et al. Host Galaxy Properties and Offset Distributions of Fast Radio Bursts: Implications for Their Progenitors. *Astrophys. J.* **2020**, *903*, 152. [CrossRef]

98. Pleunis, Z.; Good, D.C.; Kaspi, V.M.; Mckinven, R.; Ransom, S.M.; Scholz, P.; Bandura, K.; Bhardwaj, M.; Boyle, P.J.; Brar, C.; et al. Fast Radio Burst Morphology in the First CHIME/FRB Catalog. *Astrophys. J.* **2021**, *923*, 1. [CrossRef]
99. Marcote, B.; Nimmo, K.; Hessels, J.W.T.; Tendulkar, S.P.; Bassa, C.G.; Paragi, Z.; Keimpema, A.; Bhardwaj, M.; Karuppusamy, R.; Kaspi, V.M.; et al. A repeating fast radio burst source localized to a nearby spiral galaxy. *Nature* **2020**, *577*, 190–194. [CrossRef]
100. Piro, L.; Bruni, G.; Troja, E.; O'Connor, B.; Panessa, F.; Ricci, R.; Zhang, B.; Burgay, M.; Dichiara, S.; Lee, K.J.; et al. The fast radio burst FRB 20201124A in a star-forming region: Constraints to the progenitor and multiwavelength counterparts. *Astron. Astrophys.* **2021**, *656*, L15. [CrossRef]
101. Bhardwaj, M.; Gaensler, B.M.; Kaspi, V.M.; Landecker, T.L.; Mckinven, R.; Michilli, D.; Pleunis, Z.; Tendulkar, S.P.; Andersen, B.C.; Boyle, P.J.; et al. A Nearby Repeating Fast Radio Burst in the Direction of M81. *Astrophys. J. Lett.* **2021**, *910*, L18. [CrossRef]
102. Ravi, V.; Law, C.J.; Li, D.; Aggarwal, K.; Burke-Spolaor, S.; Connor, L.; Lazio, T.J.W.; Simard, D.; Somalwar, J.; Tendulkar, S.P. The host galaxy and persistent radio counterpart of FRB 20201124A. *arXiv* **2021**, arXiv:2106.09710.
103. Bhandari, S.; Heintz, K.E.; Aggarwal, K.; Marnoch, L.; Day, C.K.; Sydnor, J.; Burke-Spolaor, S.; Law, C.J.; Xavier Prochaska, J.; Tejos, N.; et al. Characterizing the Fast Radio Burst Host Galaxy Population and its Connection to Transients in the Local and Extragalactic Universe. *Astron. J.* **2022**, *163*, 69. [CrossRef]
104. Caleb, M.; Spitler, L.G.; Stappers, B.W. One or several populations of fast radio burst sources? *Nat. Astron.* **2018**, *2*, 839–841. [CrossRef]
105. Palaniswamy, D.; Li, Y.; Zhang, B. Are There Multiple Populations of Fast Radio Bursts? *Astrophys. J.* **2018**, *854*, L12. [CrossRef]
106. Hessels, J.W.T.; Spitler, L.G.; Seymour, A.D.; Cordes, J.M.; Michilli, D.; Lynch, R.S.; Gourdji, K.; Archibald, A.M.; Bassa, C.G.; Bower, G.C.; et al. FRB 121102 Bursts Show Complex Time-Frequency Structure. *Astrophys. J. Lett.* **2019**, *876*, L23. [CrossRef]
107. Nimmo, K.; Hessels, J.W.T.; Keimpema, A.; Archibald, A.M.; Cordes, J.M.; Karuppusamy, R.; Kirsten, F.; Li, D.Z.; Marcote, B.; Paragi, Z. Highly polarized microstructure from the repeating FRB 20180916B. *Nat. Astron.* **2021**, *5*, 594–603. [CrossRef]
108. CHIME/FRB Collaboration; Amiri, M.; Andersen, B.C.; Bandura, K.M.; Bhardwaj, M.; Boyle, P.J.; Brar, C.; Chawla, P.; Chen, T.; Cliche, J.F.; et al. Periodic activity from a fast radio burst source. *Nature* **2020**, *582*, 351–355. [CrossRef]
109. Rajwade, K.M.; Mickaliger, M.B.; Stappers, B.W.; Morello, V.; Agarwal, D.; Bassa, C.G.; Breton, R.P.; Caleb, M.; Karastergiou, A.; Keane, E.F.; et al. Possible periodic activity in the repeating FRB 121102. *Mon. Not. R. Astron. Soc.* **2020**, *495*, 3551–3558. [CrossRef]
110. Cruces, M.; Spitler, L.G.; Scholz, P.; Lynch, R.; Seymour, A.; Hessels, J.W.T.; Gouiffés, C.; Hilmarsson, G.H.; Kramer, M.; Munjal, S. Repeating behaviour of FRB 121102: Periodicity, waiting times, and energy distribution. *Mon. Not. R. Astron. Soc.* **2021**, *500*, 448–463. [CrossRef]